Dynamic scaling theory of the critical attenuation and dispersion of sound in a classical fluid: The binary liquid

Richard A. Ferrell
Center for Theoretical Physics, Department of Physics and Astronomy, University of Maryland, College Park, Maryland 20742

Jayanta K. Bhattacharjee
Department of Physics, Indian Institute of Technology, Kanpur 208016, India
(Received 13 August 1984)

Following the ideas of Herzfeld, Rice, Fixman, and Mistura, we are able to establish the adiabatic temperature oscillations as the sole origin of the critical attenuation and dispersion near the consolute point of a binary liquid. Special attention is given to the scaling function $F(\Omega)$ for the attenuation normalized to its consolute-point value, where Ω is the frequency, scaled by the relaxation rate of the fluid. By imposing some general conditions, we are led to the empirical function $F(\Omega)=(1+\Omega^{-1/2})^{-2}$, which is in excellent agreement with the data of Garland and Sanchez. By including a new hydrodynamic effect, we find that the frequency scale is also in accord with experiment.

I. INTRODUCTION

On December 23, 1816, Pierre Simon Laplace[1] read a paper before the Academie Française in Paris on the propagation of sound in air. He showed that the error in Newton's calculation of the velocity of sound resulted from the neglect of the local temperature changes generated by the rapid compressions and dilations of the gas. In modern language, Laplace's contribution was the demonstration that agreement with experiment is achieved when the sound velocity is calculated from the adiabatic rather than from the isothermal compressibility. The adiabatic temperature rise upon compression increases the effective stiffness of the air, thereby removing the 20% discrepancy in Newton's calculation of the sound velocity. The adiabatic temperature oscillations play an essential role, not only in the propagation of sound, but also in the attenuation of sound in polyatomic gases, as noted by Herzfeld and Rice.[2] They noted that the transfer of energy from the translational degrees of freedom to the internal degrees of freedom (i.e., the vibrational modes of oscillation of the molecules), is characterized in general by various mean relaxation times τ_i. When the sound frequency ω equals one of the τ_i's, the excitation of the corresponding internal mode will lag behind the temperature oscillation, as measured in the translational modes. The resulting hysteresis can be described by a complex frequency-dependent specific heat,[3] leading in turn to a complex and frequency-dependent compressibility and propagation velocity. The imaginary part of the velocity corresponds to the ultrasonic attenuation coefficient α.

Fixman[4] and Mistura[5] applied the Herzfeld-Rice idea to second-order phase transitions of classical fluids. In this case the "internal modes" can be considered to be the continuum of long-wavelength order-parameter fluctuations. The relaxation times in a fluid are normally very short. But the critical slowing down occurring in the vicinity of a second-order phase transition brings the relaxation rates τ_i^{-1} of the long-wavelength modes down into the experimentally accessible frequency range. By adding the idea of dynamic scaling[6] to the Herzfeld-Rice-Fixman-Mistura approach, the present authors[7] have found excellent quantitative agreement between theory and experiment for ultrasonic attenuation near the λ point of liquid He^4. The present paper is an effort to provide a thorough discussion of the same type of theory for the binary liquid, with a subsequent similar paper to be devoted to the pure fluid.[8]

The Herzfeld-Rice mechanism for ultrasonic attenuation in the binary liquid 3-methylpentane and nitroethane has been verified by Clerke *et al.*[9] By means of sudden adiabatic pressure changes it was possible[10] to measure the "coupling constant." This is the proportionality constant that relates the amplitude of the adiabatic temperature oscillation to the amplitude of the pressure oscillation. The numerical value of the coupling constant permitted an unambiguous prediction of the strength of the ultrasonic attenuation in the same binary mixture. We contend that the exact agreement, within experimental error, with the measurements of Harada *et al.*[11] establishes that our theory is based on the correct physical mechanism. The theories of Kawasaki,[12] of Shiwa and Kawasaki,[13] and of Kroll and Ruhland[14] differ from ours in that they attempt to calculate the second viscosity (or "bulk" viscosity) coefficient directly.[15]

In order to compare with the experimentally observed temperature dependence of the ultrasonic attenuation it is necessary that the theory provide a scaling function for the frequency-dependent specific heat. The present paper constitutes a refinement of our earlier calculation of the scaling function.[16] The scaling function is characterized by the following two parameters: (1) a for the frequency

scale and (2) b for the shape. In Sec. IV and in Appendixes A and B we establish that, because of a new hydrodynamic effect, the value of a is smaller than calculated in Ref. 16. By carrying out the specific-heat calculation to two loop order we find a value of b somewhat greater than before. Both of these changes seem to find confirmation in the recent measurements of Garland and Sanchez,[17] as illustrated in Figs. 5–7.

In the present treatment we derive various general conditions that have to be satisfied by the attenuation function $F(\Omega)=\alpha_\lambda/\alpha_\lambda^c$, where α_λ is the ultrasonic attenuation per wavelength, α_λ^c is its value at the critical point, and Ω is a certain scaled frequency. A new finding is that the empirical function $F(\Omega)=(1+\Omega^{-1/2})^{-2}$ satisfies all of the imposed conditions, as well as giving an excellent fit to the data, as shown in Figs. 5 and 6. The simplicity of this form of $F(\Omega)$ facilitates the comparison of ultrasonic attenuation data with the theory.

Section II is a review of the thermodynamic basis of our theory and leads directly into the simple critical-point frequency dependence that is discussed in Sec. III. Section IV deals with the more complicated problem of the scaling function and concludes with a detailed comparison of the empirical function with the data of Garland and Sanchez.[17] Section V deals with various aspects of the dispersion in the ultrasonic velocity. Here we not only make use of the Kramers-Kronig relations but, in addition, present a new treatment of dispersion based on the Cauchy-Riemann conditions that have to be satisfied by any function of a complex variable (in this case, the frequency-dependent specific heat). Section VI is primarily of academic interest and discusses the underlying distribution of relaxing modes that gives rise to the observed frequency-dependent specific heat. Section VII is a brief summary followed by Appendix A, dealing with the Kawasaki scaling function for the order-parameter relaxation, and Appendix B, dealing with the ϵ expansion, including a short discussion of the effect of the new hydrodynamic effect on the frequency scale parameter a.

II. THERMODYNAMICS

In this section we study the thermodynamic behavior of the propagation velocity u of low-frequency and long-wavelength sound in the vicinity of the critical point. This will provide a sound basis for the calculation of the more complicated, but closely related, effects of attenuation and dispersion in Secs. III–V. Because we are concerned with pressure changes, it is necessary to consider not just one critical point but, rather, a "λ line" of critical points described by the pressure-dependent critical temperature $T_c(P)$. In the specific case of the binary liquid 3-methylpentane + nitroethane, for example, this function has been measured by Beysens and Tufeu[18] over a wide range of pressure and by Clerke *et al.*,[9,10] with greater accuracy over a more limited pressure range. In principle, the variation of the critical concentration with pressure also needs to be taken into account. But we will neglect this pressure dependence here because it is known empirically to be very small in most binary liquids. Furthermore, we have found[19] that even in cases where there is an appreciable critical-concentration pressure dependence, this has a negligible net effect on sound propagation.

In the critical region, it is useful to employ as temperature variable the displacement away from the λ line

$$\Delta T=T-T_c(P)\ . \tag{2.1}$$

For sound propagation we need to know how the volume V varies with P, under the clamping condition of constant entropy S. Referring all extensive thermodynamic variables to unit mass of the fluid, we find V from the Gibbs function by

$$V=\left[\frac{\partial G}{\partial P}\right]_T=\left[\frac{\partial G}{\partial P}\right]_{\Delta T}+\left[\frac{\partial G}{\partial \Delta T}\right]_P\left[\frac{\partial \Delta T}{\partial P}\right]_T$$
$$=\left[\frac{\partial G}{\partial P}\right]_{\Delta T}+T_c' S\ . \tag{2.2}$$

The prime denotes differentiation with respect to P. Integrating away from the λ line at constant pressure gives

$$G(P,\Delta T)=G_c(P)-\int_0^{\Delta T} S(P,\Delta T')d\Delta T'\ , \tag{2.3}$$

where $G_c(P)\equiv G(P,0)$ is the Gibbs function at points on the λ line. The required derivative parallel to the λ line and at constant displacement ΔT from it is therefore

$$\left[\frac{\partial G}{\partial P}\right]_{\Delta T}=G_c'-\int_0^{\Delta T}\frac{\partial S(P,\Delta T')}{\partial P}d\Delta T'\simeq G_c'-S_c'\,\Delta T\ , \tag{2.4}$$

where we have approximated $(\partial S/\partial P)_{\Delta T}$ by its value along the λ line and have taken it outside the integral. Substituting Eq. (2.4) into (2.2), we obtain the desired result

$$V(P,\Delta T)=G_c'+T_c' S-S_c'\,\Delta T\ . \tag{2.5}$$

The isentropic compressibility β_S is therefore given by

$$-V\beta_S=\left[\frac{\partial V}{\partial P}\right]_S=\left[\frac{\partial V}{\partial P}\right]_S^c+T_c''\Delta S-S_c''\Delta T$$
$$-S_c'\left[\frac{\partial \Delta T}{\partial P}\right]_S\ , \tag{2.6}$$

with the λ-line limit expressed as

$$-V\beta_S^c=\left[\frac{\partial V}{\partial P}\right]_S^c=G_c''+T_c''S_c\ . \tag{2.7}$$

Here we will neglect the first-order terms in ΔT and $\Delta S\equiv S-S_c$ in Eq. (2.6), although in the similar case[20,21] of the propagation of sound in superfluid He^4 they have to be included. With this simplification, the isentropic compressibility becomes

$$\beta_S=\beta_S^c+\frac{S_c'}{V_c}\left[\frac{\partial \Delta T}{\partial P}\right]_S\ . \tag{2.8}$$

The adiabatic temperature variation is expressed by

$$\left[\frac{\partial \Delta T}{\partial P}\right]_S = -\frac{(\partial S/\partial P)_{\Delta T}}{(\partial S/\partial \Delta T)_P} \simeq -\frac{T_c S_c'}{C_P} = -g\frac{V_c}{C_P} , \quad (2.9)$$

where we have again approximated the entropy derivative by its λ-line value. The dimensionless coupling constant

$$g = \frac{T_c S_c'}{V_c} \quad (2.10)$$

has been determined to be $g = -0.34 \pm 0.01$ in 3-methylpentane + nitroethane.[9] Substituting Eqs. (2.9) and (2.10) into Eq. (2.8) yields

$$\beta_S = \beta_S^c - \frac{V_c}{T_c}\frac{g^2}{C_P} , \quad (2.11)$$

a quantity that has been measured directly by Tanaka *et al.*[22] The sound velocity is given by

$$u^{-2} = u_c^{-2} - \frac{g^2}{T_c C_P} , \quad (2.12)$$

where u_c is the velocity at the critical point. Because g enters squared, Eq. (2.12) represents a decreasing linear function of C_P^{-1} for all binary fluids, as illustrated schematically by Fig. 1, regardless of the sign of g. The second term on the right-hand side of Eq. (2.12) is generally small compared to u_c^{-2}, which permits Eq. (2.12) to be approximated by

$$u = u_c + \frac{g^2 u_c^3}{2T_c C_P} . \quad (2.13)$$

This increasing linear function of C_P^{-1} is identical in form to the expression used by Barmatz and Rudnick[23] for sound propagation[21] near the λ transition in liquid He^4. Because of the equivalence of Eqs. (2.12) and (2.13), we call Fig. 1 a "Barmatz-Rudnick plot."

All of the above analysis can be carried through at a finite frequency ω for an input pressure signal with time dependence $\exp -i\omega t$. Equations (2.11)—(2.13) then relate the frequency-dependent specific heat $\tilde{C}_P(\omega)$ to the frequency-dependent compressibility $\tilde{\beta}_S(\omega)$ and the frequency-dependent velocity $\tilde{u}(\omega)$. Thus Eqs. (2.13) and (2.11) become

$$\tilde{u}(\omega) = u_c + \frac{g^2 u_c^3}{2T_c \tilde{C}_P(\omega)} \quad (2.14)$$

and

$$\tilde{\beta}_S(\omega) = \beta_S^c - \frac{V_c}{T_c}\frac{g^2}{\tilde{C}_P(\omega)} . \quad (2.15)$$

The frequency dependence is studied in detail in Secs. III—V. In this section we limit ourselves to the first deviation of these functions from their thermodynamic zero-frequency limiting values of $\tilde{C}_P(0) = C_P$, $\tilde{\beta}_S(0) = \beta_S$, and $\tilde{u}(0) = u$. We split $\tilde{C}_P(\omega)$ up into its noncritical frequency-independent background component C_1 and the critical part $C(\omega)$, so $C_P = C_1 + C(0)$. A two-term low-frequency Taylor's expansion for $C(\omega)$ gives

$$C(\omega) \simeq C(0) + \omega C'(0) = C(0)(1 + i\omega\tau) , \quad (2.16)$$

where we define an effective mean relaxation time by

$$\tau = -i\frac{C'(0)}{C(0)} . \quad (2.17)$$

From Eqs. (2.15) and (2.16) the $\omega\tau \ll 1$ correction to Eq. (2.11) becomes

$$\tilde{\beta}_S(\omega) = \beta_S + iC(0)\frac{V_c}{T_c}\left[\frac{g}{C_P}\right]^2 \omega\tau . \quad (2.18)$$

The imaginary part of $\tilde{\beta}_S(\omega)$ corresponds to a lagging response and, thus, a hysteresis and damping of the sound waves. In the low-frequency regime the damping can alternatively be described within the framework of conventional hydrodynamics by the introduction of the bulk viscosity η', which gives

$$\beta_S(\omega) = \beta_S + i\eta'\beta_S^2\omega . \quad (2.19)$$

Identification of the imaginary terms in Eqs. (2.18) and (2.19) yields

$$\eta' = C(0)\frac{V_c}{T_c}\left[\frac{g}{\beta_S C_P}\right]^2 \tau . \quad (2.20)$$

The dominant temperature dependence in Eq. (2.19) is provided by τ, the other factors being more slowly varying. It needs to be emphasized, as already discussed by Herzfeld and Litovitz[15] for ultrasonic attenuation in polyatomic gases, that *the concept of a bulk viscosity has been introduced only for the purpose of establishing contact with conventional hydrodynamics. η' is of no value in elucidating the physical mechanism of the damping, which depends upon the adiabatic temperature variation,* as exhibited by the second term of Eq. (2.15).

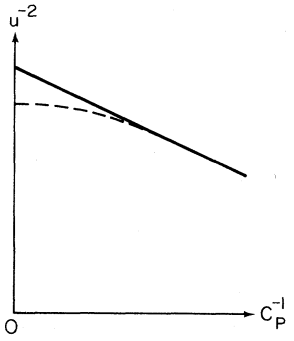

FIG. 1. u^{-2} vs C_P^{-1} where u is the velocity of sound and C_P the specific heat at constant pressure. The straight-line Barmatz-Rudnick plot is the thermodynamic relation. The dashed curve shows the deviation from thermodynamics produced by a finite frequency, resulting in frequency dependence at the critical point.

III. DYNAMIC SCALING AT THE CRITICAL POINT

The critical part of the specific heat that determines the complex sound velocity via Eq. (2.14) has the thermodynamic temperature dependence

$$C(0) \propto t^{-\alpha_0}, \tag{3.1}$$

where α_0 is the critical exponent and $t=\Delta T/T_c=(T-T_c)/T_c$ is the reduced temperature. The critical diffusion that produces the relaxation of the concentration fluctuations[24,25] is determined by

$$D=\frac{k_B T}{6\pi\eta\xi}, \tag{3.2}$$

where k_B is Boltzmann's constant, η is the shear viscosity, and ξ is the correlation length with the critical exponent ν. The characteristic relaxation rate for the fluid is therefore

$$\gamma(t)=2D\xi^{-2}=\gamma_0 t^{z_0\nu}=\tilde{\gamma}_0(\Delta T)^{z_0\nu}, \tag{3.3}$$

where, with the critical viscosity exponent included,

$$z_0=3.05 . \tag{3.4}$$

γ_0 and $\tilde{\gamma}_0$ are constants. For 3-methylpentane + nitroethane and with ΔT in kelvins,

$$\frac{\tilde{\gamma}_0}{2\pi}=0.33 \text{ MHz} . \tag{3.5}$$

Using Eq. (3.3) to eliminate t in terms of γ, we can express the temperature dependence of $C(0)$ in the entirely equivalent form

$$C(\gamma,0) \propto \gamma^{-\alpha_0/z_0\nu}, \tag{3.6}$$

where the small exponent is

$$\frac{\alpha_0}{z_0\nu}=\frac{0.11}{3.05\times 0.63}=0.057 . \tag{3.7}$$

When we pass to the critical point, dynamic scaling, as exhibited explicitly by the single-loop expressions of Sec. IV, requires that γ be replaced by $-i\omega/a$, where a is a dimensionless constant of order 1. Thus, with $t=0$ and $\gamma=0$ Eq. (3.6) is replaced by

$$C(0,\omega) \propto \left[\frac{-i\omega}{a}\right]^{-\alpha_0/z_0\nu} . \tag{3.8}$$

Figure 2 illustrates this crossover behavior from the quasithermodynamic region I, where γ is the dominant variable, to the nonthermodynamic region II, where the frequency dominates and γ disappears from the problem. The dashed slanting line at $\omega=a\gamma$ divides the two regions. An experiment at constant ω, as indicated by the horizontal dot-dashed line, passes from region I to region II as the critical point is approached.

The factor $-i$ that occurs in Eq. (3.8) is required by the purely relaxational nature of the critical-concentration fluctuations. It has the important consequence that $\tilde{C}_P(\omega)$ is a complex function leading, in turn, by virtue of Eq. (2.14), to a complex sound velocity. The attenuation coefficient α in Np/cm is proportional to

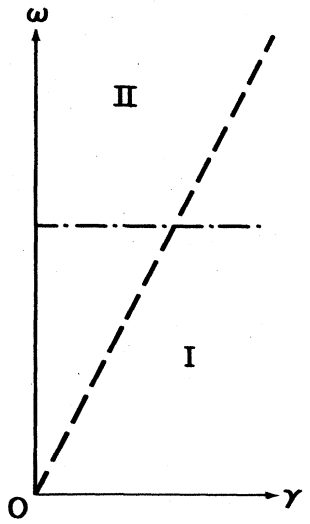

FIG. 2. Frequency and rate plane illustrating the working of dynamic scaling. Crossover occurs from quasithermodynamic to nonthermodynamic behavior at the dashed line $\omega=a\gamma$. As the critical point is approached at a constant finite frequency ω' as shown by the dot-dashed line, γ dependence changes to ω dependence.

$$\begin{aligned}\omega \,\mathrm{Im}\tilde{C}_P(\omega)^{-1} &\simeq \frac{-\omega}{(\mathrm{Re}\tilde{C}_P)^2}\mathrm{Im}C(0,\omega)\\ &=\frac{-\omega^2}{a(\mathrm{Re}\tilde{C}_P)^2}\left[\frac{a}{\omega}\right]^{1+\alpha_0/z_0\nu}\sin\left[\frac{\alpha_0\pi}{2z_0\nu}\right]\\ &\simeq\frac{-\alpha_0\pi}{2z_0\nu a}\frac{\omega^2}{(\mathrm{Re}\tilde{C}_P)^2}\left[\frac{a}{\omega}\right]^{1+\alpha_0/z_0\nu},\end{aligned} \tag{3.9}$$

the approximations being permitted by $\alpha_0/z_0\nu \ll 1$. The noncritical background attenuation varies as ω^2, so that a plot of α/ω^2 versus $\omega^{-1-\alpha_0/z_0\nu}=\omega^{-1.06}$ will be a straight line, provided that the frequency dependence of $\mathrm{Re}\tilde{C}_P$ can be neglected. We note that this approximation is not, in fact, allowed, for the special case of 3-methylpentane + nitroethane, where the effective exponent in the observable frequency range is expected to be 1.03 instead of 1.06. We further comment in passing that, by keeping the various numerical factors in Eq. (3.9), it has been possible to verify[9] that Eq. (2.15) predicts exactly the observed strength of the attenuation at the critical point.

IV. DYNAMIC SCALING FUNCTION

A. Decoupled-mode specific heat

In Sec. III above we limited our study of the frequency-dependent specific heat $C(\gamma,\omega)$ to the γ and ω axes where

$$C(\gamma,0) \propto \gamma^{-\alpha_0/z_0\nu} \tag{4.1a}$$

and

$$C(0,\omega) \propto \left[\frac{-i\omega}{a}\right]^{-\alpha_0/z_0\nu} \tag{4.1b}$$

are the thermodynamic and critical-point functions, respectively. In this section we take up the study of $C(\gamma,\omega)$ in the entire positive quadrant of the γ-ω plane, as illustrated in Fig. 2. Equations (4.1a) and (4.1b) constitute "boundary conditions" that must be satisfied by any theoretical expression for $C(\gamma,\omega)$. It is convenient to consider the ratio of $C(\gamma,\omega)$ to $C(\gamma,0)$, the thermodynamic limit, so that the boundary condition of Eq. (4.1b) becomes the asymptotic equality

$$\frac{C(\gamma,\omega)}{C(\gamma,0)} \sim \left[\frac{z}{a}\right]^{-\alpha_0/z_0\nu} \tag{4.2}$$

for $|z| \gg 1$, where

$$z \equiv -i\Omega \equiv -i\frac{\omega}{\gamma} . \tag{4.3}$$

Thus a is a scale parameter for the reduced frequency Ω. In order to compare various approximations for $C(\gamma,\omega)$ it is convenient to eliminate the occurrence of the critical exponent α_0 by defining the scaling function

$$L(z) \equiv \frac{z_0\nu}{\alpha_0} \ln\left[\frac{C(\gamma,\omega)}{C(\gamma,0)}\right] . \tag{4.4}$$

The boundary condition of Eq. (4.1a) for the thermodynamic limit becomes

$$L(0) = 0 , \tag{4.5a}$$

whereas the critical-point limit, Eq. (4.1b), is transformed into the asymptotic condition

$$L(z) \sim -\ln(z/a) \tag{4.5b}$$

for $|z| \gg 1$. In addition to the frequency-scale parameter a, it is possible from the low-frequency behavior of $L(z)$ to define a shape parameter b by

$$b \equiv -a\left.\frac{dL(z)}{dz}\right|_{z=0} . \tag{4.6}$$

Because the critical fluctuations are not able to follow a variable temperature signal, the frequency dependence generally reduces $C(\gamma,\omega)$ below its thermodynamic equilibrium value $C(\gamma,0)$. In fact, $L(z)$ is a negative and monotonically decreasing function of z along the positive real z axis, i.e., along the positive imaginary Ω axis. Elsewhere in the complex z plane, $L(z)$ is a complex quantity. Along the real Ω axis, i.e., the negative imaginary z axis, we define the attenuation function, as discussed below in Sec. IV B, by

$$F(\Omega) \equiv \frac{2}{\pi} \mathrm{Im} L(-i\Omega) , \tag{4.7}$$

normalized at the critical point to $F(\infty) = 1$. The 50% attenuation frequency $\Omega_{1/2}$, defined by

$$F(\Omega_{1/2}) \equiv \tfrac{1}{2} , \tag{4.8}$$

provides an alternative frequency-scale parameter and is equivalent to a.

We now turn to the decoupled-mode computation of the frequency-dependent specific heat via the correlation function for $\delta\phi^2$, the fluctuation of the squared order parameter. We denote the order parameter at space-time point $\mathbf{x}_1$ and t_1 in a classical fluid by $\phi(1)$. This fluctuating order parameter will describe the entropy and concentration fluctuations in a pure fluid or binary liquid, respectively. $\delta\phi^2$ is essentially the energy fluctuation. As is well known in the theory of thermodynamic fluctuations, the latter is related to the specific heat. We begin with the correlation function for $\delta\phi^2$ at a time difference of $t_{21} = t_2 - t_1$. Because the individual components of wave number p decay at the pair rate $\gamma(p,\kappa)$, we have the desired correlation function in the decoupled-mode formalism, represented by the single noninteracting loop of Fig. 3(a), in the form

$$G_2(t_{21}) = \tfrac{1}{2}\int d^D x_{21} \langle \delta\phi^2(2)\delta\phi^2(1)\rangle = \frac{1}{(2\pi)^D}\int d^D p\, e^{-\gamma(p,\kappa)|t_{21}|} g^2(p,\kappa) . \tag{4.9}$$

For the order-parameter correlation function we use the Ornstein-Zernike approximation

$$g(p,\kappa) = \frac{1}{\kappa^2 + p^2} = \frac{\kappa^{-2}}{1+q^2} , \tag{4.10}$$

where we have introduced the scaled wave number

$$q = \frac{p}{\kappa} . \tag{4.11}$$

[The Fisher-Langer modification of $g(p,\kappa)$ for $q \gg 1$ will be discussed in Sec. IV B below.] For $p \ll \kappa$ (long-wavelength limit) the pair rate is related to the characteristic rate $\gamma(t)$ by $\gamma(p,\kappa) = (p/\kappa)^2\gamma(t)$.

The frequency-dependent specific heat is, according to the fluctuation-dissipation theorem, the Fourier transform of the causal linear-response function

$$R(t) = -\frac{d}{dt}\{[G_2(t) - G_2(0)]\Theta(t)\} , \tag{4.12}$$

where

$$\Theta(t) = \begin{cases} 1, & t > 0 \\ 0, & t < 0 \end{cases} \tag{4.13}$$

is the usual retarded unit step function. It follows that

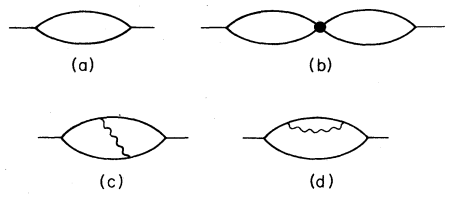

FIG. 3. Specific-heat graphs to two-loop order. The wavy lines in (c) and (d) correspond to the hydrodynamic shear modes.

$$C(\gamma,\omega)=G_2(0)+i\omega g_2(\omega)\ , \tag{4.14}$$

where the Fourier transform of the correlation function is

$$g_2(\omega)=\int_0^\infty dt\, e^{i\omega t}G_2(t)=\int_0^\infty dt\, e^{-z\gamma t}G_2(t)\ , \tag{4.15}$$

with the second version becoming the Laplace transform for real z. Carrying out the Laplace transform on the integrand of Eq. (4.9) gives

$$-z\gamma\int_0^\infty e^{-\gamma(p,\kappa)t}e^{-z\gamma t}dt=\frac{-z\gamma}{z\gamma+\gamma(p,\kappa)}=\frac{-z}{z+\Gamma_{D'}(q)}\ , \tag{4.16}$$

where the scaled-pair decay rate is

$$\Gamma_{D'}(q)\equiv\frac{\gamma(p,\kappa)}{\gamma(t)}=q^2(1+q^2)^{D'/2-1}\ . \tag{4.17}$$

For the actual three-dimensional fluid, setting $D'=3$ in Eq. (4.17) gives a good approximation to the Kawasaki function,[24] as discussed in Appendix A. For mathematical convenience, however, it is useful to treat D' as a free parameter. We note that Eq. (4.17) implies $z_0=D'$, which is equivalent to neglecting the weak critical divergence of the viscosity. For the purpose of obtaining an approximation to the scaling function, this is sufficiently accurate.

With these preliminaries behind us, we can now substitute Eqs. (4.17), (4.16), and (4.9) into Eqs. (4.15) and (4.14) to obtain, with $\epsilon\equiv 4-D$,

$$C(\gamma,\omega)=\frac{C_D}{(2\pi)^D}\kappa^{-\epsilon}H_{DD'}(z)\ , \tag{4.18}$$

where

$$\frac{1}{D}C_D=\frac{\pi^{D/2}}{\left[\frac{D}{2}\right]!} \tag{4.19}$$

is the volume of the unit sphere in D dimensions, and

$$H_{DD'}(z)=\frac{1}{C_D}\int d^Dq\frac{1}{(1+q^2)^2}\frac{\Gamma_D'(q)}{z+\Gamma_{D'}(q)}=\int_0^\infty dq\frac{q^{D-1}}{(1+q^2)^2}\frac{\Gamma_D'(q)}{z+\Gamma_{D'}(q)}\ . \tag{4.20}$$

In the thermodynamic limit the "dynamic dimensionality" D' disappears from Eq. (4.20). We therefore drop this index and, with the variable substitution $u=q^2$, obtain

$$H_D=\tfrac{1}{2}\int_0^\infty du\frac{1}{(1+u)^2}u^{D/2-1}=\tfrac{1}{2}\pi\frac{1-\epsilon/2}{\sin(\pi\epsilon/2)}\ . \tag{4.21}$$

By inspection of Eq. (4.18) we identify the critical exponent for the single-loop model as

$$\alpha_0=\epsilon\nu\ . \tag{4.22}$$

Substituting Eqs. (4.22) and (4.20) into Eq. (4.4) gives the scaling function

$$L(z)=\frac{D'}{\epsilon}\ln\left[\frac{H_{DD'}(z)}{H_D}\right]\ . \tag{4.23}$$

With the denominator in Eq. (4.23) given by Eq. (4.21), it remains only to obtain an expression for the integral in Eq. (4.20) as a function of z. This can be carried out in closed form in the high-frequency limit, which will lead to an explicit formula for the frequency-scale parameter a. Substituting the $q\gg 1$ asymptotic form of Eq. (4.17),

$$\Gamma_{D'}(q)\sim q^{D'}\ , \tag{4.24}$$

into Eq. (4.20) gives

$$H_{DD'}^{\rm hf}(z)=\frac{1}{D'}\int_0^\infty du\frac{1}{(z+u)u^{\epsilon/D'}}=\frac{1}{D'}I\left[\frac{\epsilon}{D'}\right]z^{-\epsilon/D'}\ , \tag{4.25}$$

where

$$I(\delta)\equiv\int_0^\infty du\frac{1}{1+u}u^{-\delta}=\frac{\pi}{\sin(\pi\delta)}\ . \tag{4.26}$$

Thus,

$$H_{DD'}^{\rm hf}(z)=\frac{\pi/D'}{\sin(\pi\epsilon/D')}z^{-\epsilon/D'}\ . \tag{4.27}$$

Substitution into Eq. (4.23) and comparison with Eq. (4.5b) yields

$$\ln a_{DD'}=\frac{D'}{\epsilon}\ln\left[\frac{4}{D'(D-2)}\frac{\sin[\pi(D/2-1)]}{\sin(\pi\epsilon/D')}\right]\ . \tag{4.28}$$

Of particular interest is the case of $D\to 4$, or $\epsilon\to 0$. Then the limiting value of ϵ^{-1} times the logarithm is $\frac{1}{2}$, independent of D'. Therefore

$$a_{4D'}=e^{D'/2}\ . \tag{4.29}$$

Special cases are

$$a_{44}=e^2=7.39\ , \tag{4.30a}$$

$$a_{43}=e^{3/2}=4.48\ , \tag{4.30b}$$

and

$$a_{32}=e=2.72\ . \tag{4.30c}$$

Appendix B is devoted to an expansion of Eq. (4.28) in powers of ϵ and $\epsilon'\equiv 4-D'$. Other special cases of Eq. (4.28) for integer values of D and D' are

$$a_{34}=2^2=4.00\ , \tag{4.30d}$$

$$a_{33}=\left[\frac{8}{3\sqrt{3}}\right]^3=3.65\ , \tag{4.30e}$$

$$a_{32}=2^2=4.00\ , \tag{4.30f}$$

$$a_{24}=(\tfrac{1}{2}\pi)^2=2.47\ , \tag{4.30g}$$

and

$$a_{23}=\left[\frac{4\pi}{3\sqrt{3}}\right]^{3/4}=3.76\ . \tag{4.30h}$$

For $D=4$, Eqs. (4.30a)—(4.30c) exhibit a steady trend of decreasing frequency scale as D' decreases. For $D=3$ the dependence on D' is much reduced and exhibits a

minimum in the vicinity of $D'=3$, as is evident in Eqs. (4.30d)–(4.30f). For $D=2$, the trend is reversed and $a_{22}=\infty$, indicating a breakdown of Eq. (4.25). This infrared divergence is discussed in Appendix B. We now take up the dependence of the shape parameter $b_{DD'}$ on the dimensionalities. The substitution of Eq. (4.23) into Eq. (4.6) gives

$$\frac{b_{DD'}}{a_{DD'}}=\frac{-D'H'_{DD'}(0)}{\epsilon H_D} \tag{4.31}$$

with the prime indicating the differentiation of the integral in Eq. (4.20). The resulting integral is readily evaluated to yield for the numerator in Eq. (4.31)

$$-D'H'_{DD'}(0)=\Gamma\left[1-\frac{\epsilon}{2}\right]\frac{\Gamma(2+\frac{1}{2}(D'-D))}{\Gamma(\frac{1}{2}D')} . \tag{4.32}$$

The denominator is found from Eq. (4.21) to be

$$\epsilon H_D=\left[1-\frac{\epsilon}{2}\right]\frac{\pi\epsilon/2}{\sin(\pi\epsilon/2)} . \tag{4.33}$$

Both of these expressions have limiting values of unity at $D=4$ and $\epsilon=0$, thereby establishing the identity

$$b_{4D'}=a_{4D'} . \tag{4.34}$$

From Eqs. (4.30a)–(4.30c) we obtain

$$b_{44}=7.39 , \tag{4.35a}$$

$$b_{43}=4.48 , \tag{4.35b}$$

$$b_{42}=2.72 . \tag{4.35c}$$

For $D=3$, Eq. (4.31) develops a D' dependence which, combined with Eqs. (4.30d)–(4.30f), yields

$$b_{34}=12.00 , \tag{4.35d}$$

$$b_{33}=9.29 , \tag{4.35e}$$

and

$$b_{32}=8.00 . \tag{4.35f}$$

Our interest is primarily in the fully three-dimensional case $D=D'=3$ for which Eqs. (4.30e) and (4.35e) give $a_{33}=3.65$ and $b_{33}=9.29$, respectively. Unfortunately, for this particular case, it is not feasible to carry out the integration and to exhibit $L_{33}(z)$ in closed form. For this reason we have determined the parameters for the frequency scale and the shapes as functions of D and D'. We will return to the scale parameter in Sec. IV C below and concentrate, for the moment, on the shape parameter. It is our experience that $b_{DD'}$ goes a long way in fixing not only the low-frequency behavior, but, in fact, the entire global shape of $L_{DD'}(z)$ over the entire range of z. It is therefore a considerable mathematical convenience that we can approximate the 33 case by other cases whose $b_{DD'}$ values are close to $b_{33}=9.29$. The integration of Eq. (4.20) is possible in terms of elementary functions for 44, 34, and 32. Thus we find, by substituting into Eq. (4.23),

$$L_{44}(z)=-\ln z+2+\frac{1}{z}\ln z+2\left[\frac{1}{z}-3\right]P(z) , \tag{4.36}$$

where

$$P(z)=\tfrac{1}{2}(1-4z)^{-1/2}\ln\left[\frac{1+(1-4z)^{1/2}}{1-(1-4z)^{1/2}}\right] , \tag{4.37}$$

and

$$L_{32}(z)=2\ln(2z^{3/2}-3z+1)-4\ln(z-1) . \tag{4.38}$$

Some care needs to be exercised in evaluating $P(z)$ in the complex plane. Along the positive real z axis, $P(z)$ is real and equal to

$$P(z)=|4z-1|^{-1/2}\times\begin{cases}\tanh^{-1}(1-4z), & 0\le z\le\frac{1}{4}\\ \tan^{-1}(4z-1), & \frac{1}{4}\le z .\end{cases} \tag{4.39}$$

By factoring the denominator of the integrand of Eq. (4.20), we can also obtain $H_{34}(z)$ in closed form. But the resulting scaling function is complicated and not convenient to use, and, therefore, will not be exhibited here. For demonstrating the close similarities that exist among the various scaling functions, in spite of their apparent differences in form, $L_{44}(z)$ and $L_{32}(z)$ will suffice.

It is a complicated, but straightforward, task to find the attenuation function according to Eq. (4.7) by extracting the imaginary part of $L_{44}(z)$ for the negative imaginary values $z=-i\Omega$. We have exhibited the resulting function $F_{44}(\Omega)$ in Fig. 2 of Ref. 6. It has a smooth monotonic rise between $F_{44}(0)=0$ and $F_{44}(\infty)=1$, with the halfway point falling at $\Omega_{1/2}^{(44)}=5.47$. Relative to the frequency-scale parameter, this is

$$\frac{\Omega_{1/2}^{(44)}}{a_{44}}=0.740 . \tag{4.40}$$

The high-frequency behavior of the scaling function is described by the three-term expansion

$$L_{44}(z)\sim-\ln z+2-\frac{3\pi}{2}z^{-1/2} , \tag{4.41}$$

where, by inspection, we recognize $a_{44}=e^2$, in agreement with Eq. (4.30a). Equations (4.7) and (4.41) give

$$F_{44}(\Omega)\simeq 1-\frac{3}{\sqrt{2}}\Omega^{-1/2}=1-b'_{44}\left[\frac{a_{44}}{\Omega}\right]^{1/2} , \tag{4.42}$$

where

$$b'_{44}=\frac{3}{e\sqrt{2}}=0.780 \tag{4.43}$$

is a shape parameter based on the high instead of the low-frequency behavior. Equation (4.42) yields quite accurately the first 20% drop in $F_{44}(\Omega)$ below $F_{44}(\infty)=1$.

The corresponding expansion for the 32 case is

$$L_{32}(z)\sim-\ln z+2\ln 2-3z^{-1/2} , \tag{4.44}$$

which yields

$$F_{32}(\Omega)\simeq 1-\frac{3\sqrt{2}}{\pi}\Omega^{-1/2}=1-b'_{32}\left[\frac{a_{32}}{\Omega}\right]^{1/2}, \tag{4.45}$$

where

$$b'_{32}=\frac{3}{\pi\sqrt{2}}=0.675\ . \tag{4.46}$$

The fact that b'_{32} differs from b'_{44} by only 14% is consistent with the near equality of b_{32} and b_{44}, for which the difference is 8%. This serves to support our contention that one parameter (either b or b') suffices to give a reasonably faithful indication of the shape of $F(\Omega)$. A further example of this is our plot of $F_{42}(\Omega)$ in Fig. 2 of Ref. 6. It is evident by comparing it with the curve for $F_{44}(\Omega)$ that the former is much steeper. This is precisely what is to be expected from the smaller value of b [2.72 as compared to 7.39, according to Eqs. (4.35c) and (4.35a)]. In Ref. 6 we advocated the preference of F_{43} over F_{44} because one of the dimensionalities had been reduced to the physically true value of 3. We now believe that this intermediate case does not give a good scaling function and that it is necessary to set *both* D and D' equal to 3. This second step of reducing D from 4 to 3 doubles the shape parameter, as seen from Eqs. (4.35b) and (4.35e). The resulting stronger low-frequency tail will stretch out the plot of $F_{33}(\Omega)$ versus Ω and result in a less-steep rise. Because b_{32} is close to b_{33}, we expect $F_{32}(\Omega)$ to be a fair representation of $F_{33}(\Omega)$. As already explained, this approximation is dictated by mathematical convenience.

The full course of the 32 attenuation function is given by

$$F_{32}(\Omega)=\frac{4}{\pi}\tan^{-1}\left[\frac{3\Omega-\sqrt{2}\Omega^{3/2}}{1-\sqrt{2}\Omega^{3/2}}\right]-\frac{8}{\pi}\tan^{-1}\Omega \tag{4.47}$$

from which we recover Eq. (4.45) for $\Omega\gg 1$ as well as

$$F_{32}\simeq\frac{4}{\pi}\Omega=\frac{2}{\pi}\frac{b_{32}}{a_{32}}\Omega \tag{4.48}$$

for $\Omega\ll 1$, in agreement with Eqs. (4.30f) and (4.35f). In order to exhibit clearly the high-frequency behavior of Eq. (4.45) we have plotted $F_{32}(\Omega)$ of Eq. (4.47) versus $(a_{32}/\Omega)^{1/2}$ as the dashed curve in Fig. 4. In this way the high-frequency variation is converted into a straight line. The halfway point falls at $\Omega_{1/2}^{(32)}=3.19$, or in units of the frequency-scale parameter $a_{32}=4$, at

$$\frac{\Omega_{1/2}^{(32)}}{a_{32}}=0.797\ . \tag{4.49}$$

The close agreement with Eq. (4.40) is to be expected from the near equality of the shape parameters.

This completes our study of the decoupled-mode theory of the frequency-dependent specific heat. The decoupling neglects the interaction of the fluctuations. In Sec. IV B we argue that, guided by the two-term ϵ expansion, we do not expect the scaling function to be modified significantly by the interactions.

B. General theory

In this subsection we discuss some theoretical aspects of the frequency-dependent specific heat that have some generality beyond the specific single-loop prototypes studied in Sec. IV A. The latter correspond to Fig. 3(a). We first turn our attention to the effect of the interaction of the fluctuations as illustrated in Fig. 3(b). We write the single-loop function as

$$C'=\frac{z_0\nu}{\alpha_0}(C-1)\ , \tag{4.50a}$$

where we write the function that has been calculated in Sec. IV A in the exponentiated form

$$C=\exp\left[\frac{\alpha_0}{z_0\nu}K\right]\ . \tag{4.50b}$$

The subtraction inside the parentheses represents the noncritical background term resulting from the Debye cutoff at short wavelengths that we have, up to now, been ignoring. The temperature and frequency-dependent function in the exponent is related to the scaling function defined in Eq. (4.4) by

$$K(\gamma,\omega)=K_{\rm TH}+L(z)\ , \tag{4.51}$$

where the substitution of $K_{\rm TH}\equiv K(\gamma,0)$ into Eq. (4.50b) yields the thermodynamic specific heat $C(\gamma,0)$. Working close to $D=4$ we have $\alpha_0=0(\epsilon)$, which permits the development in powers of α_0 according to

$$C'=K+\frac{\alpha_0}{2z_0\nu}K^2+\cdots\ . \tag{4.52}$$

Now representing the strength of the first-order interaction of the fluctuations by $-u_4$, corresponding to the heavy dot in Fig. 3(b), the effect of the fluctuations on the specific heat is given to this accuracy by the modified function

$$\begin{aligned}C''=C'-u_4C'^2&=K+\left[\frac{\alpha_0}{2z_0\nu}-u_4\right]K^2+\cdots\\&=K+\frac{\alpha_0'}{2z_0\nu}K^2+\cdots\\&\simeq\frac{z_0\nu}{\alpha_0'}(e^{(\alpha_0'/z_0\nu)K}-1)\\&=\frac{z_0\nu}{\alpha_0'}C^{\alpha_0'/\alpha_0}-\text{const}\ .\end{aligned} \tag{4.53}$$

Because Eq. (4.51) is still applicable, it follows from Eq. (4.53) that the scaling function is unaffected by the fluctuations to first order in the ϵ expansion. To this order, the only effect of the fluctuations is to change the critical specific-heat exponent from its "bare" single-loop value to

$$\alpha_0'=\alpha_0-2z\nu u_4\ . \tag{4.54}$$

This is, of course, the standard ϵ expansion theory of α_0 and tends to explain why the observed value at $D=3$ of 0.11 is much smaller than the single-loop value of $\nu=0.63$. Our purpose in repeating this well-known theoretical result here is to establish qualitatively the justification for neglecting the effect of the static interaction

of the fluctuations on the scaling functions. This is the basis for our approximation of using the single-loop functions derived in Sec. IV A.

The ultrasonic attenuation is determined by $\mathrm{Im}C''$. By substituting Eq. (4.51) into Eq. (4.50) and exploiting $\alpha_0'/z_0\nu \ll 1$ and the fact that Im L is bounded by $\frac{1}{2}\pi$ we obtain

$$\mathrm{Im}C'' \propto \exp\left[\frac{\alpha_0'}{z_0\nu}(K_{\mathrm{TH}}+\mathrm{Re}L)\right]\mathrm{Im}L \ . \tag{4.55}$$

By comparing the attenuation per wavelength α_λ with its critical value α_λ^c and neglecting the weak dispersion and the slow variation of the prefactor in Eq. (4.55), we find for their ratio

$$\frac{\alpha_\lambda}{\alpha_\lambda^c}=\frac{2}{\pi}\mathrm{Im}L=F(\Omega) \ , \tag{4.56}$$

the definition of the attenuation function in Eq. (4.7). In subsequent work we drop the prime on α_0 and the double prime on C.

A second general feature of the scaling function is the error ensuing in the single-loop integral of Eq. (4.20) from the use of the Ornstein-Zernike approximation, which has its high-momentum behavior

$$g(p,\kappa)\simeq p^{-2}Q(q) \tag{4.57a}$$

described by the deviation function

$$Q(q)=1-q^{-2} \ . \tag{4.57b}$$

The correct high-momentum behavior is known[26] to be

$$g(p,\kappa) \propto p^{-2+\eta}Q(q) \ , \tag{4.57c}$$

with the deviation function

$$\begin{aligned} Q(q)&=1-C_1q^{-1/\nu}-C_2q^{-(1-\alpha)/\nu} \\ &\simeq 1-C_{F-L}q^{-(2-\alpha)/2\nu} \\ &=1-C_{F-L}q^{-D'/2} \ . \end{aligned} \tag{4.58}$$

Here we have neglected the small anomalous dimension exponent η and have approximated the two terms by a single effective Fisher-Langer coefficient and an average exponent, which has been simplified by the scaling law

$$2-\alpha=D'\nu \ . \tag{4.59}$$

(Because C_1 and C_2 are of opposite sign, an average exponent with different weighting would be more accurate.) Substituting Eq. (4.58) into the integrand of Eq. (4.20) yields a correction to its high-frequency value which can be calculated as a weighted average. Denoting this average with angular brackets, and noting that the variable $q^{D'}$ is converted into z by the averaging, gives the fractional correction to Eq. (4.25) of

$$\langle Q(q)\rangle-1 \propto -C_{F-L}z^{-1/2} \ . \tag{4.60}$$

This requires that the attenuation have, in general, the high-frequency form

$$F(\Omega)\simeq 1-\mathrm{const}\Omega^{-1/2} \ . \tag{4.61}$$

It is very convenient that, in spite of the lack of an explicit Fisher-Langer correction, the general requirement expressed by Eq. (4.61) is nevertheless satisfied by F_{44} and F_{32}, as is evident in Eqs. (4.42) and (4.45), respectively. Being just part of the interaction effect, Eq. (4.60) is only suggestive, with a 3-loop calculation still needed.

We now study in greater detail the low-frequency behavior of the single-loop integral. The frequency-dependent factor in the integrand of Eq. (4.20) is

$$\begin{aligned} \frac{\Gamma_{D'}}{z+\Gamma_{D'}}&=1-\frac{z}{\Gamma_{D'}}+\frac{z^2}{\Gamma_{D'}(\Gamma_{D'}+z)} \\ &\simeq 1-\frac{z}{\Gamma_{D'}}+\frac{z^2}{q^2(q^2+z)} \ , \end{aligned} \tag{4.62}$$

where we have substituted the $q \ll 1$ approximation to Eq. (4.17) in the last term. Substitution of Eq. (4.62) into Eq. (4.20) yields

$$\begin{aligned} H_{3D'}(z)&=H_3-zH_{3D'}'(0)+z^2\int_0^\infty dq\frac{q^2}{(1+q^2)^2}\frac{1}{\Gamma_{D'}(\Gamma_{D'}+z)} \\ &\simeq H_3-zH_{3D'}'(0)+z^2\int_0^\infty dq\frac{1}{q^2+z} \\ &=H_3-zH_{3D'}'(0)+\tfrac{1}{2}\pi z^{3/2} \ . \end{aligned} \tag{4.63}$$

Substituted into Eqs. (4.23) and (4.7), this gives the low-frequency forms for the scaling and attenuation functions

$$L_{3D'}(z)\simeq -\frac{b_{3D'}}{a_{3D'}}z+2D'z^{3/2} \tag{4.64}$$

and

$$\begin{aligned} F_{3D'}(\Omega)&\simeq\frac{2}{\pi}\frac{b_{3D'}}{a_{3D'}}\Omega-\frac{2\sqrt{2}}{\pi}D'\Omega^{3/2} \\ &=\frac{2}{\pi}\frac{b_{3D'}}{a_{3D'}}\Omega-0.90D'\Omega^{3/2} \ . \end{aligned} \tag{4.65}$$

These equations are a refinement on the low-frequency linear behavior studied in Sec. IV A and characterized by the shape parameter $b_{DD'}$. The $\Omega^{3/2}$ correction to the linear term results from the $D=3$ nature of phase space and must be regarded as a general requirement that has to be satisfied by any theory for $F(\Omega)$. For this reason $F_{44}(\Omega)$ has to be regarded as less satisfactory than $F_{32}(\Omega)$. We note that for $\Omega \ll 1$, Eq. (4.47) reduces to

$$F_{32}(\Omega)\simeq\frac{4}{\pi}\Omega-\frac{4\sqrt{2}}{\pi}\Omega^{3/2}=\frac{4}{\pi}\Omega-1.80\Omega^{3/2} \ , \tag{4.66}$$

in accord with Eq. (4.65). With $D'=3$, the coefficient of $\Omega^{3/2}$ in Eq. (4.65) becomes -2.70.

We conclude this section by considering the possibility of characterizing the scaling function entirely on the basis of $F(\Omega)$. In other words, suppose $F(\Omega)$ is given without the underlying scaling function $L(z)$. The shape parameters b and b' are determined by the low- and high-frequency behavior of $F(\Omega)$, respectively. But for this we need to know the value of a which, according to the discussion of Sec. III, is determined from the high-frequency form of K by

$$K_{\rm hf}(\gamma,i\gamma z)\,|_{z=a}=K(\gamma,0)\ . \tag{4.67}$$

In Sec. V below we use the Kramers-Kronig relations to express K as an integral over $F(\Omega)$. Substituting this result for $K(\gamma,0)$ into Eq. (4.67) leads to

$$\ln a=\lim_{\Omega_D\to\infty}\left[\ln\Omega_D-\int_0^{\Omega_D}d\Omega\,\frac{F(\Omega)}{\Omega}\right] \tag{4.68}$$

which can alternatively be written as

$$\int_0^\infty\frac{d\Omega}{\Omega}[F(\Omega)-\Theta(\Omega-a)]=0\ , \tag{4.69}$$

with the unit step function defined in Eq. (4.13). From Eq. (4.69) we see that a can be interpreted as the position of a sharp cutoff that would be equivalent to the smoothly varying function $F(\Omega)$.

C. Empirical attenuation function

As argued in Sec. IV B, the decoupled-mode single-loop integral, in spite of its neglect of the interaction of the fluctuations, yields correctly the scaling and attenuation functions. These functions are not affected, at least to first order in the ϵ expansion, by the interaction. Therefore we should, in principle, base our theory on $L_{33}(z)$ and $F_{33}(\Omega)$, as defined by Eqs. (4.23), (4.20), and (4.7). But we deviate from this straightforward course for the following two reasons: (1) mathematical convenience, and (2) uncertain accuracy of the ϵ expansion. For both of these reasons it is preferable not to adhere strictly to the 33 single-loop result, but rather to characterize it in a more general fashion by the frequency parameter a and by the various low- and high-frequency shape parameters. Because of reason (2) above, a function $F(\Omega)$ satisfying the several general conditions can be expected to have as much validity as the specific function $F_{33}(\Omega)$. Furthermore, by a judicious choice of form, $F(\Omega)$ may be much easier to work with, because of the impossibility of carrying out the 33 single-loop integration in closed form. Such a function exhibiting all of the necessary and desirable features is

$$F(\Omega)=\left[1+\frac{1}{\sqrt{\Omega}}\right]^{-2}=\frac{\Omega}{(1+\sqrt{\Omega})^2}\ . \tag{4.70}$$

Carrying out the integration in Eq. (4.68) shows that the frequency-scale parameter for this function is

$$a=e^2=7.39\ . \tag{4.71}$$

The half-attenuation point comes at

$$\Omega_{1/2}=3+2\sqrt{2}=5.83\ , \tag{4.72}$$

with the ratio

$$\frac{\Omega_{1/2}}{a}=0.789 \tag{4.73}$$

only 1% removed from the value 0.797 found for the 32 case. The low-frequency expansion of Eq. (4.70) is

$$F(\Omega)\simeq\Omega-2\Omega^{3/2}=\frac{2}{\pi}\frac{\pi}{2}e^2\frac{\Omega}{a}-2\Omega^{3/2}$$
$$=\frac{2}{\pi}\frac{\pi}{2}e^2\frac{\Omega}{a}-2e^3\left[\frac{\Omega}{a}\right]^{3/2}\ , \tag{4.74}$$

where use has been made of Eq. (4.71). The coefficient of the linear term yields the shape parameter

$$b=\frac{\pi}{2}e^2=11.6\ . \tag{4.75}$$

This value of b is close to the predicted value of 10.7 for b_{33} from Eq. (4.35e), after inclusion of the 15% correction from Appendix A. Thus Eq. (4.70) acquires a further quantitative basis from the theory over and above the qualitative requirements that led to its choice. The second term in Eq. (4.74) has the general form required by Eq. (4.65), with the coefficient of -2 as compared to the *a priori* value of -2.70.

In the high-frequency-range, Eq. (4.70) becomes

$$F(\Omega)\simeq 1-2\Omega^{-1/2}=1-\frac{2}{e}\left[\frac{a}{\Omega}\right]^{1/2}\ , \tag{4.76}$$

which yields the shape parameter

$$b'=\frac{2}{e}=0.736\ . \tag{4.77}$$

This value is in the good range and is bracketed by the results $b'_{44}=0.780$ and $b'_{32}=0.675$ [as reported in Eqs. (4.42) and (4.46), respectively]. Thus we see that the shape parameters for Eq. (4.70) correspond well to those coming from the single-loop integrals, but that the a value of Eq. (4.71) is bigger than that coming from the $D=3$ integrals. This latter defect is readily eliminated by a scale change so that the empirical attenuation function, adjusted for any desired value of a, or half-attenuation frequency $\Omega_{1/2}$, is

$$F(\Omega)=\left[1+\frac{1}{e}\left[\frac{a}{\Omega}\right]^{1/2}\right]^{-2}$$
$$=\left[1+0.414\left[\frac{\Omega_{1/2}}{\Omega}\right]^{1/2}\right]^{-2}\ . \tag{4.78}$$

Obviously the shape parameters are unaffected by this scale change. The coefficient of $\Omega^{3/2}$ in Eq. (4.74) is, however, raised to

$$-2\frac{e^3}{\sqrt{a^3}}=-5.76\ , \tag{4.79}$$

or somewhat more than twice the *a priori* expected value of -2.70. Equation (4.78), as a function of $(a/\Omega)^{1/2}$, has been plotted as the solid curve in Fig. 4. As expected from the approximate equality of b' and b'_{32}, there is no appreciable separation of the solid and dashed curves in the high-frequency region. This is evident in the upper portion of these curves, where the salient feature is the linear or nearly linear dependence on $\Omega^{-1/2}$ for the first (20–30)% drop. The curves cross at approximately the half-attenuation point, with F_{32} lying below F for larger values of $\Omega^{-1/2}$, as expected from the smaller shape pa-

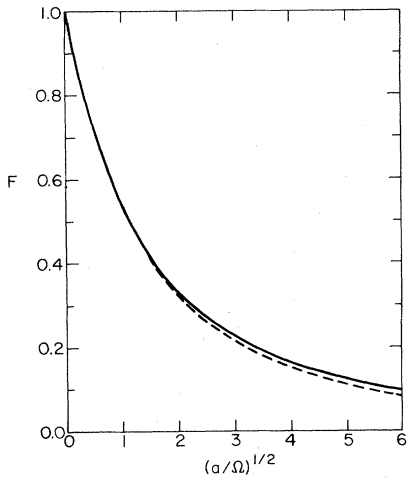

FIG. 4. Normalized attenuation function $F(\Omega)$ vs $(a/\Omega)^{1/2}$, where Ω is the scaled frequency.

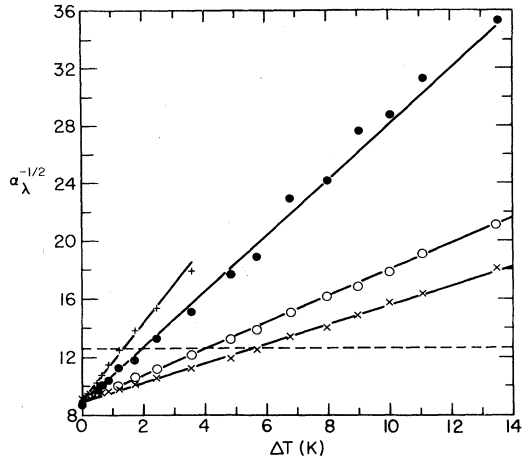

FIG. 5. Attenuation per wavelength α_λ vs ΔT, measured by Garland and Sanchez (Ref. 17) at the following frequencies in MHz: 1(+), 3(●), 9(○), 17(×).

rameter ($b_{32}=8$ as compared with $b=11.6$).

The comparison of Eq. (4.78) with experimental measurements of α_λ, the attenuation per wavelength, is most easily carried out for $F^{-1/2}$, which is a completely linear function of $\Omega^{-1/2}$. Therefore, identifying $(\alpha_\lambda/\alpha_\lambda^c)^{-1/2}$ with $F^{-1/2}$, where α_λ^c is the critical-point value of α_λ, we expect a straight-line plot for

$$\left[\frac{\alpha_\lambda}{\alpha_\lambda^c}\right]^{-1/2} = [F(\Omega)]^{-1/2} = 1+0.414\left[\frac{\Omega_{1/2}}{\Omega}\right]^{1/2}$$
$$= 1+0.414\left[\frac{\Omega_{1/2}}{\omega}\right]^{1/2}\gamma^{1/2}$$
$$= 1+0.414\left[\frac{\tilde{\gamma}_0\Omega_{1/2}}{\omega}\right]^{1/2}(\Delta T)^{0.96}$$
$$= 1+0.414\left[\frac{\Delta T}{\Delta T_{1/2}}\right]^{0.96} \simeq 1+C_{1/2}\,\Delta T\ , \tag{4.80}$$

where

$$C_{1/2} \equiv \frac{0.414}{\Delta T_{1/2}}\ . \tag{4.81}$$

Although a straight line is to be expected when the data are plotted versus $\Delta T^{0.96}$, it is more convenient to make the plot versus ΔT instead. The 4% difference in exponent produces a negligible curvature. In any case, the error from this approximation vanishes at $\Delta T=\Delta T_{1/2}$, the half-attenuation temperature. The latter is related to the half-attenuation frequency by

$$\Omega_{1/2} = \frac{\omega}{\tilde{\gamma}_0}(\Delta T_{1/2})^{-1.93}\ . \tag{4.82}$$

(Here it is not permitted to approximate the exponent.)

Figure 5 shows the 1, 3, 9, and 17 MHz data of Garland and Sanchez,[17] plotted in the manner of Eq. (4.80). To avoid cluttering the plot, we have omitted the 9 and 11 MHz runs, as well as some of the data points close to $\Delta T=0$. For every run, there is a straight line that gives a good fit to the data. In order to find the best overall fit for each frequency, we do not give any special weight to the critical-point attenuation. Consequently, the quantity α_λ^c in Eq. (4.80) is an effective critical-point attenuation which may differ by a few percent from the value actually measured at $T=T_c$. For example, at 3 and 17 MHz, the effective value of α_λ^c from the best fit is found to be 0.0126 in both cases. The corresponding measured values are 0.0132 and 0.0119, respectively. (The noncritical background has been subtracted from all of the data shown in Fig. 5.) In fact, we find the same effective value of α_λ^c for all of the frequencies. Because of this convenient circumstance, all of the straight lines have the same vertical axis intercept, $(\alpha_\lambda^c)^{-1/2}=8.9$. For each particular frequency, the slope of the straight line, $(\alpha_\lambda^c)^{-1/2}C_{1/2}$, determines $T_{1/2}$ according to Eq. (4.81). This construction is shown by the horizontal dashed line, at $\sqrt{2}(\alpha_\lambda^c)^{-1/2}=12.6$. When the straight line crosses the dashed line the attenuation falls to 50% of its (effective) critical-point value. The values of $\Delta T_{1/2}$ from these crossings yield the values of $\Omega_{1/2}$ that are discussed in the next paragraph.

The 3 MHz run of Garland and Sanchez has a special status. As is evident in Fig. 5, for this frequency these authors have succeeded in carrying the measurements of $\alpha_\lambda(\Omega)$ out to especially small values of Ω. Figure 6 compares its data with Eq. (4.78) in a more conventional way, namely, as $\alpha_\lambda/\alpha_\lambda^c$ plotted versus $\log_{10}\Omega$. There is evidently good agreement with the empirical function shown as the curve. Here, for the vertical axis normalization we continue to use the effective value of α_λ^c which, as noted above, is 5% below the actual value. For the horizontal axis normalization we obtain $\Delta T_{1/2}=1.93$ from the intersection of the solid and dashed lines in Fig. 5. With this value and $\tilde{\gamma}_0/2\pi=0.333$ MHz substituted into Eq. (4.82) we find $\Omega_{1/2}=2.53$. This result and the determinations of

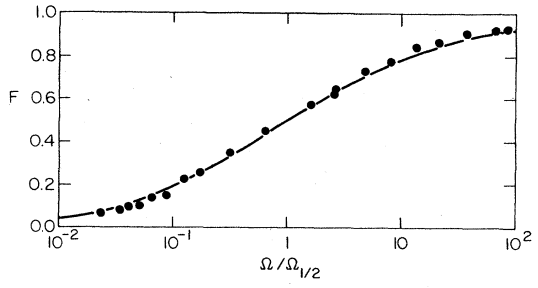

FIG. 6. Normalized attenuation function $F(\Omega)$ vs $\Omega/\Omega_{1/2}$. $\Omega_{1/2}$ is the value of the dimensionless frequency Ω for which $F(\Omega)=\frac{1}{2}$.

$\Omega_{1/2}$ at the other frequencies are exhibited in Fig. 7 as a function of the frequency f (in MHz). Giving extra weight to the 3 MHz run we find a mean value of approximately $\Omega_{1/2}=2.0$, as indicated by the horizontal dashed line in Fig. 6.

We conclude this section by confronting our theoretical prediction of $\Omega_{1/2}$ with the above experimental value of 2.0. From Eq. (4.30e) and the 18% enhancement discussed in Appendix A, we expect $a=(3\pi/8)a_{33}=1.18\times 3.65=4.31$, which would yield $\Omega_{1/2}=3.40$, by virtue of Eq. (4.73). There would seem to be a serious discrepancy between this result and the observed value, smaller by about 40%. Some important physical effect has evidently been left out of the calculation. We believe that we have been able to identify the missing effect in the critical relaxation process itself. The usual critical relaxation of an order-parameter fluctuation is illustrated by Fig. 3(d). This is taken into account by Eq. (4.17) and by the discussion in Sec. III and in Appendix A. Figure 3(c), on the other hand, illustrates a new effect ensuing from the coupling of the order-parameter modes to the transverse hydrodynamic modes, represented in the figures by the plain and wavy lines, respectively. This is a kind of exchange process that does not contribute to the decay of a single mode. It, however, has to be taken into account when dealing with the relaxation of a pair of order-parameter modes, as is the case with the frequency-dependent specific heat. The details of this calculation will be presented in a separate paper[27] devoted to the theory of the frequency-dependent specific heat. We have found that the "exchange" graph of Fig. 3(c) brings a substantial cancellation of the "direct" graph of Fig. 3(d), so that the effective decay rate is substantially smaller than that of an isolated order-parameter fluctuation. The theoretically expected frequency scale is found in Appendix B to be shifted down to $\Omega_{1/2}=2.1$, in good agreement with the experimental value of 2.0 that is shown by the dashed line in Fig. 7.

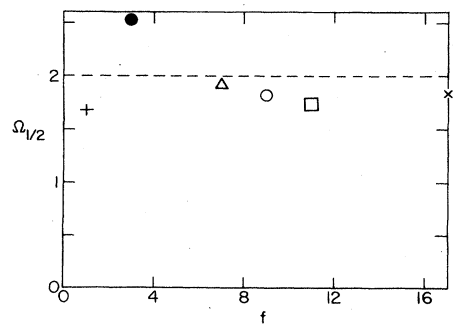

FIG. 7. $\Omega_{1/2}$ vs frequency f(MHz) from the plot in Fig. 5 of the data of Garland and Sanchez (Ref. 17). The dashed line shows the theoretical prediction.

V. DISPERSION

The dramatic increase in the attenuation of sound near the critical point is a clear manifestation of the critical slowing down of the diffusive relaxation of the concentration fluctuations. This effect is more readily accessible to experimental observation than the corresponding effect of the fluctuations on the velocity of sound. But the study of the critical dispersion is not without interest and it is to this goal that this section is devoted. It is important to recognize that, for this purpose, we no longer need a microscopic theory of the critical dynamics of the fluctuations. Because the critical attenuation has been explored so completely, we can use it as an empirical input for predicting the critical dispersion. Once we have established, as we claim to have done in Sec. IV, that the observed attenuation can be understood on the basis of the microscopic theory, we can then consider that the latter has fulfilled its task and that it can therefore be laid aside. At this point completely general considerations can take us from the observed attenuation to the associated dispersion that must inevitably go along with it. The important connection follows from the fact that $C(\omega)$ is a causal response function which is therefore analytic in the upper half of the complex frequency plane. Furthermore, since $C(\omega)$ is a superposition of relaxing modes, it has no zeros in the upper-half plane. (The regular region extends, in fact, all the way down to the cut along the negative imaginary frequency axis.) Therefore, the logarithm is also analytic in this region, which is the precondition for the applicability of the Kramers-Kronig relation connecting $L_1(\Omega)$ and $L_2(\Omega)$, the real and imaginary parts of the scaling function. As $L_2(\Omega)$ is already known from the attenuation, we thus find $L_1(\Omega)$, which determines the dispersion.

In Sec. V A below, we carry out in detail the program sketched above. An alternative derivation of $L_1(\Omega)$, based on the Cauchy-Riemann conditions, is presented in Sec. V B. Although approximate, this alternative treatment is, in fact, quite accurate and has the advantage of being simpler than the Kramers-Kronig method. The reader who is primarily interested in the results may wish to skip over this mathematical work and go directly to the applications in Secs. V C and V D.

A. Kramers-Kronig relation

As explained above, $L(z)=L(-i\Omega)=L_1(\Omega)+iL_2(\Omega)$ is a causal function which therefore satisfies the Kramers-Kronig relation

$$L_1(\Omega)=\frac{1}{\pi}\mathrm{P}\int_{-\infty}^{+\infty}d\Omega'\frac{1}{\Omega'-\Omega}L_2(\Omega')+\text{const}\ , \quad (5.1)$$

with the question of convergence at the limits of integration to be dealt with directly. By changing the principal value integral to a contour integral passing below the pole at $\Omega'=\Omega$, we include $iL_2(\Omega)$ to obtain

$$L(z)=\frac{1}{\pi}\int_{-\infty}^{+\infty}d\Omega'\frac{1}{\Omega'-iz}L_2(\Omega')+\text{const}$$
$$=\frac{2}{\pi}\int_0^{+\infty}d\Omega'\frac{\Omega'}{\Omega'^2+z^2}L_2(\Omega')+\text{const}\ . \quad (5.2)$$

Here we have invoked the fact that $L_2(\Omega')$ is an odd function. We now drop the prime from the variable of integration, identify the attenuation function as $F=(2/\pi)L_2$, and require that the constant term be such that $L(0)=0$. This puts $L(z)$ into the subtracted convergent form

$$L(z)=\int_0^{\infty}d\Omega\left[\frac{\Omega}{\Omega^2+z^2}-\frac{1}{\Omega}\right]F(\Omega)$$
$$=-z^2\int_0^{\infty}d\Omega\frac{1}{\Omega(\Omega^2+z^2)}F(\Omega)\ , \quad (5.3)$$

the first line being generally more useful than the second. It is convenient to impose a high-frequency "Debye" cutoff on the integral and to deal with the two terms of the integrand separately. In the range $|z|\gg 1$ we can use the asymptotic approximation $F\simeq 1$ in the first term to obtain

$$\int_0^{\Omega_D}d\Omega\frac{\Omega}{\Omega^2+z^2}=\ln\left[\frac{\Omega_D}{z}\right]\ . \quad (5.4)$$

Substituted into Eqs. (5.3) and (4.5), this yields

$$\ln a=\lim_{\Omega_D\to\infty}\left[\ln\Omega_D-\int_0^{\Omega_D}d\Omega\,\frac{F(\Omega)}{\Omega}\right]\ , \quad (5.5)$$

as reported in Eq. (4.68) of Sec. IV B. The integration in Eq. (5.5) is readily carried out in terms of the variable $\sqrt{\Omega}$, giving $a=e^2$ for the present case of interest [namely, the empirical function of Eq. (4.70)], as reported in Eq. (4.71). We integrate along the dashed line in Fig. 8.

The integration of Eq. (5.3) for an arbitrary value of z is straightforward and yields

$$L(z)=\frac{2z^2}{z^2+1}+z^2\frac{3-z^2}{(z^2+1)^2}\ln z$$
$$+\frac{\pi\sqrt{2}z^{3/2}}{(z^2+1)^2}(1-2z-z^2)+\tfrac{1}{2}\pi\frac{-z+3z^3}{(z^2+1)^2}\ . \quad (5.6)$$

It can readily be verified that Eq. (5.6) conforms to the various high- and low-frequency limiting forms that have been discussed above in Sec. IV. It is apparent from the plot of $L(z)$ versus $\ln(z/a)$ in Fig. 9 that it serves as a smooth interpolating function, along the lines discussed qualitatively in Sec. III above, between the thermodynamic limit $L(0)=0$ and the high-frequency asymptote $-\ln(z/a)$. The latter is shown as the dashed straight line in Fig. 9.

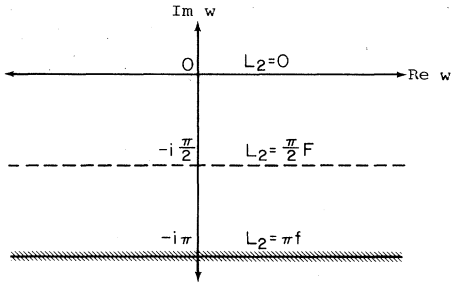

FIG. 8. The complex ω plane illustrating the definition of the attenuation function F at $\mathrm{Im}\,w=-\frac{1}{2}\pi$ and of the spectral function at $\mathrm{Im}\,w=-\pi$, where $w=\ln(-i\Omega)$.

For physical applications we have to evaluate Eq. (5.6) along the negative imaginary z axis, which is the range of physically real frequencies. It is a simple mathematical exercise to verify that along this axis $L_2(\Omega)$ reduces to $\frac{1}{2}\pi$ times the attenuation function $F(\Omega)$ of Eq. (4.70), with which we started. The corresponding dispersive, or real, part of the function is plotted in Fig. 10 and is expressed by

$$L_1(\Omega)=\frac{\Omega^2}{\Omega^2-1}\left[2-\ln\Omega-\frac{4\ln\Omega}{\Omega^2-1}\right]-\frac{\pi\Omega^{3/2}}{(\Omega+1)^2}\ . \quad (5.7a)$$

(This function is regular at $\Omega=1$, the singularity being only apparent.) For $\Omega\gg 1$ Eq. (5.7a) becomes

$$L_1(\Omega)=-\ln\Omega+2-\pi\Omega^{-1/2}\ , \quad (5.7b)$$

the coefficient of $\Omega^{-1/2}$ satisfying the general requirement that it equal $\frac{1}{2}\pi$ times the corresponding coefficient in $F(\Omega)$.

B. Cauchy-Riemann conditions

We base our work in this section also on the analyticity of the function $L(z)$ in the right half of the complex z plane. But instead of exploiting this analyticity in an integral form by means of the Kramers-Kronig relation, we use it now in a differential form which, with suitable approximations, leads to simpler expressions, of yet adequate accuracy. It is convenient to transform to the new complex variable

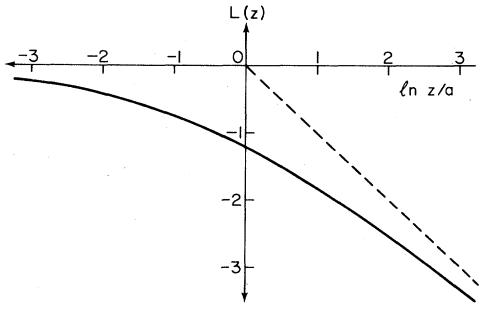

FIG. 9. Empirical scaling function $L(z)$ vs $\ln z/a$. The dashed straight line shows the asymptotic behavior for $z\gg 1$.

$$w_1+iw_2=w=\ln z\ . \tag{5.8}$$

As shown in Fig. 8, this transforms the positive z axis into the $w_1=\mathrm{Re}w$ axis, along which L is a real function. Indicating explicitly the dependence of L_1+iL_2 on the variables $w_{1,2}$, we have

$$L_2(w_1,0)=0 \tag{5.9}$$

for all w_1. The entire z plane is mapped into a horizontal ribbon of width 2π. The cut along the negative z axis is mapped into the line $w_2=\mathrm{Im}w=-\pi$, shown at the bottom of Fig. 8, and into the line $w_2=\pi$ (not shown). The line of physically real frequencies falls at $w_2=-\frac{1}{2}\pi$ as shown by the horizontal dashed line in Fig. 8. Along this line the measured attenuation function $F(\Omega)=F(e^{w_1})$ is related to the complex function L by

$$L_2(w_1,-\tfrac{1}{2}\pi)=\tfrac{1}{2}\pi F\ . \tag{5.10}$$

Because of its analyticity, L satisfies the Cauchy-Riemann conditions

$$\partial_1 L_1(w_1,w_2)=\partial_2 L_2(w_1,w_2) \tag{5.11a}$$

and

$$\partial_2 L_1(w_1,w_2)=-\partial_1 L_2(w_1,w_2)\ , \tag{5.11b}$$

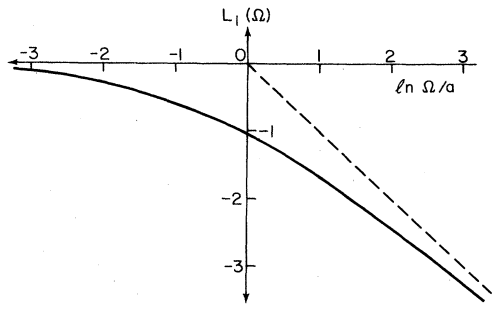

FIG. 10. $L_1(\Omega)$ vs $\ln(\Omega/a)$, where $L(z)=L_1(\Omega)+iL_2(\Omega)$. The dashed line shows the asymptotic behavior for $\Omega/a\gg 1$.

where we denote the partial differentiation $\partial/\partial w_{1,2}$ by $\partial_{1,2}$. It immediately follows that both L_1 and L_2 satisfy Laplace's equation, which gives the useful operator identity

$$\partial_2^2=-\partial_1^2\ . \tag{5.12}$$

With these preliminaries out of the way, we can now relate the scaling function defined along the w_1 axis to the measured attenuation function by working our way down from $w_2=0$ to the $w_2=-\frac{1}{2}\pi$ line, holding w_1 constant. Taylor's theorem for fixed w_1 gives

$$\begin{aligned}L_2(w_1,-\tfrac{1}{2}\pi)&=\exp(-\tfrac{1}{2}\pi\partial_2)L_2(w_1,w_2)\,|_{w_2=0}\\&=\sinh(-\tfrac{1}{2}\pi\partial_2)L_2(w_1,w_2)\,|_{w_2=0}+\cosh(-\tfrac{1}{2}\pi\partial_2)L_2(w_1,w_2)\,|_{w_2=0}\\&=\sin(-\tfrac{1}{2}\pi\partial_1)L_1(w_1,0)+\cos(-\tfrac{1}{2}\pi\partial_1)L_2(w_1,0)\ ,\end{aligned} \tag{5.13}$$

the last line ensuing from the application of Eqs. (5.11a) and (5.12). By Eq. (5.9) the last term vanishes identically yielding the desired differential connection

$$L_1(w_1,0)=\tfrac{1}{2}\pi\csc(-\tfrac{1}{2}\pi\partial_1)F\ . \tag{5.14}$$

This is a rigorous identity. We have found that approximating it by the two-term expression

$$L_1(w_1,0)=-[\partial_1^{-1}+(\pi^2/24)\partial_1]F \tag{5.15}$$

is quite accurate. The differential operator acting on $F(\Omega)$ is

$$\partial_1=\Omega\frac{\partial}{\partial\Omega} \tag{5.16a}$$

and its inverse is

$$\partial_1^{-1}=\int d\Omega\,\Omega^{-1}\ . \tag{5.16b}$$

After these operations are carried out, Ω is to be replaced by

$$w_1=\ln\Omega\ , \tag{5.17}$$

and, in turn, by z, to give, for $z>0$,

$$L(z)=-2\ln(1+z^{1/2})+\frac{2z^{1/2}}{1+z^{1/2}}-\frac{\pi^2}{24}\frac{z}{(1+z^{1/2})^3}\ , \tag{5.18}$$

For all practical purposes, Eq. (5.18) is entirely equivalent to the exact but more complicated expression, Eq. (5.6). The accuracy of Eq. (5.18) is confirmed for $z\gg 1$ by

$$L(z)\simeq-\ln z+2-\left[4+\frac{\pi^2}{24}\right]z^{-1/2}\ . \tag{5.19}$$

where the coefficient of $z^{-1/2}$ deviates by only a fraction of 1% from the exact value $\pi\sqrt{2}$. This result is to be expected from the operator identity

$$\csc(-\tfrac{1}{2}\pi\partial_1)\Omega^{\mu}=\csc(-\tfrac{1}{2}\pi\mu)\Omega^{\mu} \tag{5.20}$$

for the eigenfunction Ω^{μ} and the associated eigenvalue μ of the operator ∂_1. For $\mu=-\frac{1}{2}$ the two-term approximation to $\csc(\pi/4)$ is very close to the exact value of $\sqrt{2}$.

The two-term approximation of Eq. (5.15) is not as accurate in the low-frequency range $0<z\ll 1$. Here Eq. (5.18) gives

$$L(z)\simeq-\left[1+\frac{\pi^2}{24}\right]z \tag{5.21}$$

with a coefficient 11% smaller in magnitude than the exact value of

$$\tfrac{1}{2}\pi\csc(-\tfrac{1}{2}\pi\mu)\,|_{\mu=1}=-\tfrac{1}{2}\pi\ . \tag{5.22}$$

But this error has negligible effect because it sets in only after $L(z)$ itself has become very small. A plot of Eq. (5.18) versus $\ln(z/a)$ is indistinguishable from the exact curve shown in Fig. 8.

The derivation of the connection between $L_1(w_1,-\frac{1}{2}\pi)$ and F follows similar lines. Again we employ Taylor's theorem, coming down from the w_1 axis, to obtain

$$\begin{aligned}L_1(w_1,-\tfrac{1}{2}\pi)&=\exp(-\tfrac{1}{2}\pi\partial_2)L_1(w_1,w_2)\,|_{w_2=0}\\&=\cosh(-\tfrac{1}{2}\pi\partial_2)L_1(w_1,w_2)\,|_{w_2=0}+\sinh(-\tfrac{1}{2}\pi\partial_2)L_1(w_1,w_2)\,|_{w_2=0}\\&=\cos(-\tfrac{1}{2}\pi\partial_1)L_1(w_1,0)-\sin(-\tfrac{1}{2}\pi\partial_1)L_2(w_1,0)\ ,\end{aligned} \tag{5.23}$$

where we have used Eqs. (5.11b) and (5.12). By Eq. (5.9) the second term in Eq. (5.23) vanishes identically. Eliminating $L_1(w_1,0)$ from the remaining term by means of Eq. (5.14) yields the desired connection

$$L_1(w_1,-\tfrac{1}{2}\pi)=\tfrac{1}{2}\pi\cot(-\tfrac{1}{2}\pi\partial_1)F\simeq\left[-\partial_1^{-1}+\frac{\pi^2}{12}\partial_1\right]F\ , \tag{5.24}$$

where we have again introduced a two-term approximation. The result of carrying out the indicated operations can be written as

$$L_1(\Omega)=-2\ln(1+\sqrt{\Omega})+\Delta L_1(\Omega)\ , \tag{5.25a}$$

where

$$\Delta L_1(\Omega)=\frac{2\sqrt{\Omega}}{1+\sqrt{\Omega}}+\frac{\pi^2}{12}\frac{\Omega}{(1+\sqrt{\Omega})^3} \tag{5.25b}$$

is a monotonic function of Ω which rises from $\Delta L_1(0)=0$ to its high-frequency limit $\Delta L_1(\infty)=2$. For $\Omega\gg1$ these equations reduce to

$$L_1(\Omega)\simeq-\ln\Omega+2-\left[4-\frac{\pi^2}{12}\right]\Omega^{-1/2}\ , \tag{5.26}$$

with the coefficient of $\Omega^{-1/2}$ differing from the exact value π by 1%. Here again the approximation is not as good for $\Omega\ll1$, where Eqs. (5.25a) and (5.25b) give

$$L_1(\Omega)\simeq-\left[1-\frac{\pi^2}{12}\right]\Omega=-0.18\Omega\ . \tag{5.27}$$

The small coefficient should in fact vanish according to

$$\tfrac{1}{2}\pi\cot(-\tfrac{1}{2}\pi\mu)\,|_{\mu=1}=0\ . \tag{5.28}$$

But as with $L(z)$, the error in the low-frequency region is of no consequence because of the smallness of the function itself. For practical applications, Eqs. (5.25a) and (5.25b) are equivalent to the exact but more complicated formula of Eq. (5.7). A plot of Eq. (5.25a) versus $\ln(\Omega/a)$ shows no perceptible deviation from the exact curve exhibited in Fig. 9.

A further function of interest is the spectral function, which will be discussed further in Sec. VI below. It is defined in terms of the variable $s=-z$ on the lower side of the cut along the negative z axis by

$$f(s)=\frac{1}{\pi}\,\mathrm{Im}L(w_1,w_2)\,|_{w_2=-\pi,w_1=\ln s}\ , \tag{5.29}$$

with the limiting values $f(0)=0$ and $f(\infty)=1$. Furthermore, for $s\gg1$,

$$1-f(s)\propto s^{-1/2}\ , \tag{5.30}$$

with the coefficient of proportionality equal to π^{-1} times the coefficient of z^{-1} in $L(z)$ and equal to $2^{-1/2}$ times the coefficient of $\Omega^{-1/2}$ in $F(\Omega)$. From Eqs. (5.6) and (5.29) we find

$$f(s)=\frac{s^2(s^2-3)}{(1+s^2)^2}+\frac{\sqrt{2}s^{3/2}}{(1+s^2)^2}(1+2s-s^2)\ . \tag{5.31}$$

A simpler expression equivalent to Eq. (5.31) within the required accuracy can be obtained from the Cauchy-Riemann conditions. Replacing $\frac{1}{2}\pi$ by π in Eq. (5.13) and substituting from Eq. (5.14) gives

$$\begin{aligned}L_2(w_1,-\pi)&=\sin(-\pi\partial_1)L_1(w_1,0)\\&=2\cos(-\tfrac{1}{2}\pi\partial_1)\sin(-\tfrac{1}{2}\pi\partial_1)L_1(w_1,0)\\&=\pi\cos(-\tfrac{1}{2}\pi\partial_1)F(\Omega)\ .\end{aligned} \tag{5.32}$$

To two-term accuracy, the substitution of Eq. (5.32) into Eq. (5.29) yields

$$f(s)=F-\frac{\pi^2}{8}\partial_1^2F\ . \tag{5.33}$$

From Eq. (4.70) we have $F(s)=(1+s^{-1/2})^{-2}$ and

$$\partial_1^2F=\frac{1-\sqrt{s}/2}{(1+\sqrt{s})^2}F\ . \tag{5.34}$$

Equation (5.34) has been substituted into Eq. (5.33) and plotted in Fig. 11 versus $s/a=s/e^2$. Equation (5.34) fixes the point of inflexion of $F(s)$ considered as a function of $\ln s$ at $s=4$, for which $F(4)=\frac{4}{9}$. This is close to the halfway point, which means that the halfway points for $f(s)$ and $F(s)$ are expected to be nearly the same. This expectation is evidently borne out in Fig. 11 where $f(s)=\frac{1}{2}$ comes at a value of s close to $\Omega_{1/2}/a^2=0.79$ [from Eq. (4.73)].

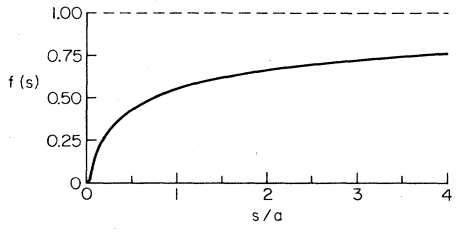

FIG. 11. The spectral function $f(s)$ vs s/a showing the distribution of relaxation rates.

For comparison we cite here the spectral functions for the single-loop specific heat in dimensionalities $DD'=44$ and 32, which are

$$f_{44}(s)=\frac{[(1+4s)^{1/2}-1]^2}{[(1+4s)^{1/2}+1](1+4s)^{1/2}} \tag{5.35}$$

and

$$f_{32}(s)=\frac{2}{\pi}\tan^{-1}\left[\frac{2s^{3/2}}{1+3s}\right], \tag{5.36}$$

respectively. When these functions are plotted versus s, there is no perceptible difference between them and $f(s)$ as expressed by either Eq. (5.34) or Eq. (5.31). In Fig. 1 of Ref. 6 we have plotted $f_{4D'}(s)$ for $D'=4$, 3, and 2. Figure 2 of Ref. 6 shows the corresponding attenuation functions $F_{4D'}(\Omega)$.

C. Differential dispersion

In experiments on the velocity of sound in a binary liquid it is generally not feasible to carry out the measurements at sufficiently low frequencies that the thermodynamic limit is attained—at least, not close to the critical point. It is, however, entirely feasible to compare sound velocities observed at different frequencies. This differential dispersion requires that we extend the theory to include the frequency derivative of the specific heat. The differential dispersion is most easily studied at the critical point, where the frequency-dependent specific heat behaves according to dynamic scaling as the simple power law

$$C\propto\omega^{-\alpha_0/z_\mu\nu}=\exp[-(\alpha_0/z_\mu\nu)\ln\omega]\ . \tag{5.37}$$

Consequently, the change in the specific heat when the frequency is changed by $\Delta\omega$ is found by differentiating Eq. (5.37), which leads to

$$\Delta C=-C\frac{\alpha_0}{z_\mu\nu}\frac{\Delta\omega}{\omega}=-C\frac{\alpha_0}{z_\mu\nu}\Delta\ln\Omega=-C\frac{\alpha_0}{z_\mu\nu}\Delta w_1\ . \tag{5.38}$$

This expression can be employed even when the frequency change is substantial because of the small value of $\alpha_0=0.11$. For example, a change in frequency by a factor of e gives $\Delta w_1=1$. Even this substantial value of Δw_1 can be treated as a small differential as far as Eq. (5.38) is concerned because of the very small numerical value of the coefficient. Thus, a change of frequency by e produces only a 5.7% change in the specific heat.

Away from the critical point, it is a simple matter to replace the logarithm in Eq. (5.37) with the scaling function $L_1(\Omega)$, defined in Eq. (5.7). But as explained in Sec. V B it is more convenient to use the two-term approximation to the Cauchy-Riemann conditions. Thus, instead of using the exact expression given in Eq. (5.7), we will calculate the differential dispersion from the simpler formula of Eq. (5.24). The fractional change in the specific heat due to $\Delta\omega$ is proportional to $\Delta\omega/\omega$ times

$$C^{-1}\partial_1 C\propto D(\Omega)\equiv-\partial_1 L_1\simeq F-\frac{\pi^2}{12}\partial_1^2 F\ . \tag{5.39}$$

This differential dispersion function, like the attenuation function, has the critical-point asymptotic limit $D(\infty)=1$. The second-derivative term is of the same form as already encountered in Eq. (5.33). Changing the coefficient by the factor $\frac{2}{3}$ and replacing s by Ω in Eq. (5.34) yields the plot of $D(\Omega)$ versus $\log_{20}(\Omega/\Omega_{1/2})$ shown in Fig. 12. As was the case with the spectral function, the halfway point for $D(\Omega)$ is practically the same as that for $F(\Omega)$. Furthermore, it is evident from comparing Fig. 6 with Fig. 12 that the two functions are quite similar over the entire range $-\infty<\log_{10}\Omega<\infty$. $D(\Omega)$ has a somewhat greater slope than $F(\Omega)$ in its middle section. At the point of inflexion, the slope is multiplied by the factor $1+\pi^2/72=1.14$, or a 14% increase. Similarly the spectral function compared to the attenuation function is steepened in its middle section by the factor $1+\pi^2/48$, or a 21% increase.

D. Velocity

In this subsection we calculate the absolute dispersion, i.e., the actual critical sound velocity as a function of frequency and temperature. This is given by the real part of Eq. (2.15). Because of

$$\mathrm{Im}\tilde{C}_P(\omega)\ll\mathrm{Re}\tilde{C}_P(\omega) \tag{5.40}$$

we can replace $\mathrm{Re}\tilde{C}_P^{-1}$ by $(\mathrm{Re}\tilde{C}_P)^{-1}$ to find

$$\mathrm{Re}\tilde{u}=u_c+\frac{g^2u_c^3}{2T_c\,\mathrm{Re}\tilde{C}_P}=u_c+\frac{g^2u_c^3}{2T_c}[C_1+\mathrm{Re}C(\gamma,\omega)]^{-1}\ . \tag{5.41}$$

Making use again of Eq. (5.40) we have from Eqs. (4.4) and (3.6)

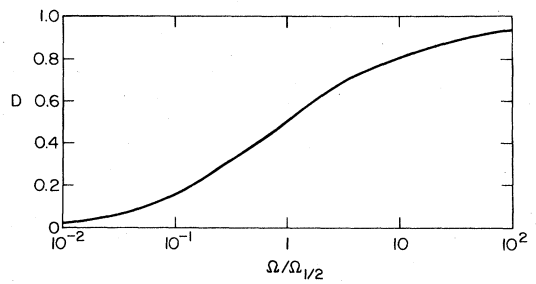

FIG. 12. Differential dispersion $D(\Omega)$ vs $\Omega/\Omega_{1/2}$.

$$\mathrm{Re}C(\gamma,\omega)=C(\gamma,0)\exp\left[\frac{\alpha_0}{z_0\nu}\mathrm{Re}L(-i\Omega)\right]$$
$$\propto\gamma^{-\alpha_0/z_0\nu}\exp\left[\frac{\alpha_0}{z_0\nu}\mathrm{Re}L(-i\Omega)\right]. \quad (5.42)$$

For $\Omega\gg1$ we can substitute from Eq. (4.5b) to obtain

$$\mathrm{Re}L(-i\Omega)=-\ln(\Omega/a) \quad (5.43)$$

so that the high-frequency limit of Eq. (5.42) becomes

$$\mathrm{Re}C(0,\omega)\propto\left[\frac{a}{\omega}\right]^{\alpha_0/z_0\nu}. \quad (5.44)$$

On the other hand, Eq. (3.8) yields

$$\mathrm{Re}C(0,\omega)\propto\left[\frac{a}{\omega}\right]^{\alpha_0/z_0\nu}\cos(\pi\alpha_0/2z_0\nu). \quad (5.45)$$

The difference between Eqs. (5.44) and (5.45) is negligible, being of second order in the small exponent $\alpha_0/z_0\nu$.

To determine the dispersion explicitly we need to substitute Eq. (5.7a) into Eq. (5.42), but a more convenient expression results from substituting the approximate formula of Eqs. (5.25a) and (5.25b). We accommodate the necessary change in the frequency scale by the introduction of the variable

$$\Omega'=\frac{e^2}{a}\Omega=\frac{e^2\omega}{a\gamma}=\frac{\omega'}{\gamma} \quad (5.46)$$

so that

$$\mathrm{Re}L(-i\Omega)=L_1(\Omega')$$
$$=-2\ln(1+\sqrt{\Omega'})+\Delta L_1(\Omega')$$
$$=\ln\gamma-2\ln(\sqrt{\gamma}+\sqrt{\omega'})+\Delta L_1(\Omega'). \quad (5.47)$$

Substituted into Eq. (5.42), this yields

$$\mathrm{Re}C(\gamma,\omega)\propto(\sqrt{\gamma}+\sqrt{\omega'})^{-2\alpha_0/z_0\nu}\exp\left[\frac{\alpha_0}{z_0\nu}\Delta L_1(\Omega')\right]$$
$$\simeq(\sqrt{\gamma}+\sqrt{\omega'})^{-2\alpha_0/z_0\nu}\left[1+\frac{\alpha_0}{z_0\nu}\Delta L_1(\Omega')\right], \quad (5.48)$$

the approximation in the last line being permitted by $\alpha_0/z_0\nu\ll1$ and by the fact that $\Delta L_1(\Omega')$ is bounded by its high-frequency limit $\Delta L_1(\infty)=2$. The scaling function contained within the large parentheses in Eq. (5.48) provides a smooth transition from the thermodynamic limit of Eq. (3.6) to the high-frequency limit of Eq. (5.44), as indicated by the dashed curve in Fig. 1.

VI. DISTRIBUTION OF RELAXATION RATES

It has long been recognized that in polyatomic gases and in many liquids the sound attenuation is not adequately described by the classical Stokes-Kirchhoff formula. The reason was shown by Herzfeld and Rice[2] to lie in the slow energy exchange between the translational and internal degrees of freedom in the polyatomic gases. The associated relaxation phenomena give rise to a frequency-dependent specific heat and thus, to an additional sound absorption. For a process characterized by a single relaxation rate $\gamma=\tau^{-1}$ the frequency-dependent component of the specific heat is

$$\tilde{C}_P(\omega)\propto(1-i\omega\tau)^{-1}. \quad (6.1)$$

If the system has several relaxation processes acting in parallel, Eq. (6.1) becomes

$$\tilde{C}_P(\omega)=\sum_j\frac{C_j}{1-i\omega\tau_j} \quad (6.2)$$

with the $\omega=0$ thermodynamic limit

$$C_P=\sum_j C_j. \quad (6.3)$$

The constants C_j are the contributions of the various individual internal modes to the thermodynamic specific heat. All of these contributions disappear from $\tilde{C}_P(\omega)$ for sufficiently high frequencies such that $\omega\gg\gamma_j=\tau_j^{-1}$, for all j. Every constant C_j is associated with a rate γ_j. Setting up this functional relationship is facilitated by analytically continuing the frequency variable down to the right-hand side of the cut along the negative imaginary axis. With $\omega=-i\sigma+\delta$, where $0\le\sigma<\infty$ and δ is an infinitesimal positive quantity, Eq. (6.2) yields

$$\mathrm{Im}\tilde{C}_P=\pi\sum_j C_j\gamma_j\delta(\sigma-\gamma_j)=\pi\sigma C(\sigma)\sum_j\delta(\sigma-\gamma_j), \quad (6.4)$$

where $C(\sigma)$ is now a continuous function of σ. At the discrete frequencies $\sigma=\gamma_i$, $C(\sigma)$ takes on the values $C(\gamma_i)=C_i$. Equation (6.4) describes the distribution of relaxation rates plotted versus the continuous rate variable σ as a set of discrete spikes at $\sigma=\gamma_i$.

The picture near the critical point of a binary liquid is conceptually the same, except for the fact that the system is characterized by a continuous set of relaxation rates $\sigma=\gamma(k,\kappa)$ belonging to the Fourier components of wave number k. Instead of a set of spikes, we now find a continuous function of σ. In the high-frequency limit $\omega/\gamma\to\infty$, Eq. (3.8) gives

$$\mathrm{Im}C(0,-i\sigma+\delta)\propto\mathrm{Im}\left[\frac{\sigma}{a}e^{-i\pi}\right]^{-\alpha_0/z_0\nu}$$
$$=\left[\frac{a}{\sigma}\right]^{\alpha_0/z_0\nu}\sin\left[\frac{\pi\alpha_0}{z_0\nu}\right]$$
$$\simeq\frac{\pi\alpha_0}{z_0\nu}\left[\frac{a}{\sigma}\right]^{\alpha_0/z_0\nu}. \quad (6.5)$$

Because the distribution of critical modes extends to short wavelengths and high relaxation rates, Eq. (6.5) is valid and nonzero out to large values of σ. At finite values of $s=\sigma/\gamma$, we have from Eq. (4.4)

$$\mathrm{Im}C(\gamma,-i\sigma+\delta)=C(\gamma,0)\mathrm{Im}e^{(\alpha_0/z_0\nu)L}$$
$$\simeq\frac{\alpha_0}{z_0\nu}C(\gamma,0)\exp\left[\frac{\alpha_0}{z_0\nu}\mathrm{Re}L\right]\mathrm{Im}L, \quad (6.6)$$

where substituting from Eq. (5.6) gives

$$\mathrm{Re}L(-s)=\frac{2s^2}{s^2+1}+\frac{s^2(3-s^2)}{(s^2+1)^2}\ln s+\tfrac{1}{2}\pi\frac{s-3s^3}{(s^2+1)^2} \tag{6.7}$$

and

$$\mathrm{Im}L(-s-i\delta)=\pi f(s)\,, \tag{6.8}$$

with the spectral function written out in Eq. (5.31). Because $f(0)=0$ and because $\mathrm{Re}L$ occurs in Eq. (6.6) with the coefficient $\alpha_0/z_0\nu\ll 1$, we can approximate Eq. (6.7) by the $s\gg 1$ asymptotic expression

$$\mathrm{Re}L(-s)\sim\ln(a/s)\,, \tag{6.9}$$

which brings Eq. (6.6) into the form

$$\mathrm{Im}C(\gamma,-i\sigma+\delta)\propto\sigma^{-\alpha_0/z_0\nu}f(\sigma/\gamma)\,. \tag{6.10}$$

The first factor produces a slow monotonic rise with decreasing σ. This is interrupted at $\sigma=0(a\gamma)$ by the opposing decrease in $f(\sigma/\gamma)$. Thus, the distribution of rates has a broad maximum and drops monotonically to zero in the range $0\le\sigma<\gamma$. In the remainder of this section we will neglect the slowly varying factor in Eq. (6.10) and concentrate on some general features of the spectral function $f(s)$, which contains the dynamic scaling information.

In arriving at the empirical attenuation function of Eq. (4.70) we did not adhere strictly to the single-loop scaling function, with its two-loop validity as established in Sec. IV B above, because of (1) mathematical convenience and (2) uncertain accuracy of the loop expansion. We argued that because of reason (2), an attenuation function $F(\Omega)$ that satisfies the various general requirements can be expected to have as much validity as the explicit single-loop function $F_{33}(\Omega)$. Analogously, we can expect that a spectral function $f(s)$ that satisfies all of the general conditions to which a spectral function is subjected may be as good an approximation to the true spectral function of the fluid as a spectral function that comes explicitly from a single-loop calculation. In other words, it is possible to exploit the basic idea of Herzfeld and Rice[2] and to set up a dynamic scaling theory of the critical ultrasonic attenuation based on an empirical distribution of relaxation rates.

In the low-momentum range, Eq. (4.17) can be approximated by

$$\Gamma_{D'}(q)\simeq q^2\,, \tag{6.11}$$

independent of D', which enables us to eliminate q as the variable of integration in the single-loop integral in terms of $\Gamma_{D'}$. Thus, for $D=3$ but D' arbitrary, the $q\ll 1$ portion of Eq. (4.20) becomes

$$\begin{aligned}\frac{1}{C_3}\int_{q\ll 1}d^3q\frac{1}{(1+q^2)^2}\frac{\Gamma_{D'}(q)}{z+\Gamma_{D'}(q)}&\simeq\frac{1}{C_3}\int_{q\ll 1}d^3q\frac{\Gamma_{D'}}{z+\Gamma_{D'}}\\&\simeq\int_{q\ll 1}dq\frac{q^4}{z+q^2}=\tfrac{1}{2}\int_{\Gamma_{D'}\ll 1}d\Gamma_{D'}\frac{\Gamma_{D'}^{3/2}}{z+\Gamma_{D'}}\,.\end{aligned} \tag{6.12}$$

Identifying $\Gamma_{D'}$ with s yields the general $D=3$ requirement for $0\le s\ll 1$,

$$f(s)\propto s^{3/2}\,. \tag{6.13}$$

Equation (6.13) is patently satisfied both by Eqs. (5.36) and (5.31) for the 32 single-loop expression and the empirical function, respectively. Equation (6.13) is illustrated by the small kink at the bottom end of the curve in Fig. 11. At the other end of the spectrum, it follows from the generalization of Eq. (4.42) that the spectral function has to be of the form

$$f(s)\simeq 1-\frac{b}{2}\left[\frac{a}{s}\right]^{1/2}\,. \tag{6.14}$$

If $f(s)$ is given, Eq. (6.8) can be inverted by means of Cauchy's theorem. An integration along the cut yields the scaling function at an arbitrary point in the complex z plane as

$$L(z)=-z\int_0^\infty\frac{ds}{s(s+z)}f(s)\,. \tag{6.15}$$

From Eq. (4.5b) and the $z\to\infty$ limit of Eq. (6.15), we determine the frequency scale by

$$\ln a=\lim_{s_D\to\infty}\left[\ln s_D-\int_0^{s_D}ds\,\frac{f(s)}{s}\right]\,, \tag{6.16}$$

similar to Eq. (4.68). Substitution of Eq. (6.15) into Eq. (4.6) yields the shape parameter

$$b=a\int_0^\infty ds\,\frac{f(s)}{s^2}\,. \tag{6.17}$$

As a simple example of the application of Eq. (6.15), we first consider the unit step function

$$f(s)=\Theta(s-1)\,. \tag{6.18}$$

Although Eq. (6.18) exhibits neither the low-frequency behavior of Eq. (6.13) nor the high-frequency behavior of Eq. (6.14), it does have the proper endpoint values $f(0)=0$ and $f(\infty)=1$. From Eqs. (6.16) and (6.17) we obtain

$$a=b=1\,. \tag{6.19}$$

Substitution of Eq. (6.18) into Eq. (6.15) gives

$$L(z)=-\ln(1+z)\,, \tag{6.20}$$

from which we obtain

$$F(\Omega)=\frac{2}{\pi}\mathrm{Im}L(-i\Omega)=\frac{2}{\pi}\tan^{-1}\Omega\,. \tag{6.21}$$

Consequently, the halfway frequency is $\Omega_{1/2}=1$, with the characteristic ratio $\Omega_{1/2}/a=1$, somewhat larger than the characteristic ratio for the single-loop scaling functions. The plot of $F(\Omega)$ versus $\ln\Omega$ shown in Fig. 6 would, in this case, have the slope corresponding to

$$\frac{dF(\Omega)}{d\ln\Omega}=\Omega F'=\frac{2}{\pi}\frac{\Omega}{1+\Omega^2}\,, \tag{6.22}$$

of $\pi^{-1}=0.32$ at $\Omega_{1/2}$. This can be compared with the

slope of the empirical function. Differentiating Eq. (4.70) gives

$$\frac{dF(\Omega)}{d\ln\Omega}=\frac{\Omega}{(1+\sqrt{\Omega})^3}\ , \tag{6.23}$$

from which we find the midpoint slope

$$\left.\frac{dF(\Omega)}{d\ln\Omega}\right|_{\Omega_{1/2}}=\frac{1}{2}-\frac{1}{2\sqrt{2}}=0.15\ . \tag{6.24}$$

The single-loop function F_{32} has a similar shape with the slightly larger midpoint slope of 0.16. The midpoint slope of twice this amount found above for the unit step function results from the abrupt jump of $f(s)$ at $s=1$ from its $f(0)$ to its $f(\infty)$ value. Therefore, the step function is an extreme case, with the slope in Eq. (6.22) providing an upper bound for the slope of any attenuation function based on a continuous spectral function.

Such a more realistic spectral function is

$$f(s)=(1-s^{-1/2})\Theta(s-1)\ . \tag{6.25}$$

This is an improvement over Eq. (6.19) in that it has the correct high-frequency behavior. From Eqs. (6.16), (6.17), and (6.14) we obtain

$$a=e^2=7.39\ , \tag{6.26a}$$

$$b=e^2/3=2.46\ , \tag{6.26b}$$

and

$$b'=\frac{\sqrt{2}}{a}=\frac{\sqrt{2}}{e}=0.521\ . \tag{6.26c}$$

Substituting Eq. (6.25) into Eq. (6.15) gives

$$L(z)=-\ln(1+z)+2-2z^{-1/2}\tan^{-1}(z^{1/2})\ , \tag{6.27}$$

so

$$\begin{aligned}\mathrm{Im}L(-i\Omega)&=\frac{2}{\pi}F(\Omega)\\&=\tan^{-1}\Omega+\frac{1}{2\sqrt{2\Omega}}\ln\left[\frac{1+\Omega+\sqrt{2\Omega}}{1+\Omega-\sqrt{2\Omega}}\right]\\&\quad-\frac{1}{\sqrt{2\Omega}}\tan^{-1}\left[\frac{\sqrt{2\Omega}}{1-\Omega}\right],\end{aligned} \tag{6.28}$$

where the arctangent is to be evaluated in the second quadrant for $\Omega>1$. For this function, the halfway point falls at $\Omega_{1/2}=5.25$, with the characteristic ratio

$$\frac{\Omega_{1/2}}{a}=\frac{5.25}{e^2}=0.71\ , \tag{6.29}$$

close to that found for the single-loop functions. The halfway slope is 0.19, smaller than that for the step spectral function. On the other hand, this slope is larger than that of Eq. (6.24) for the empirical function, which is to be expected from the relatively small values of the shape parameters in Eqs. (6.26b) and (6.26c). Although the high-frequency behavior of Eq. (6.14) is qualitatively correct, the small value of $b'=0.521$ compared to $b'=0.736$ for the empirical function indicates that the $\Omega^{-1/2}$ term is relatively weak. Thus, the decrease of $F(\Omega)$ in Eq. (6.28) from $F(\infty)=1$ down to $F(\Omega_{1/2})=\frac{1}{2}$ as Ω decreases is more confined to the midregion, which increases the midpoint slope.

As a final example of the possibility of basing a theory of critical attenuation on a postulated distribution of relaxation rates, we consider the following spectral function which has the required behavior in both the high- and low-frequency regions:

$$f(s)=(1+s^{-1/2})^{-3}\ . \tag{6.30}$$

Equations (6.16) and (6.17) give

$$a=b=e^3=20.1\ , \tag{6.31}$$

from which we find

$$b'=\left[\frac{2}{a}\right]^{1/2}=\sqrt{2}e^{-3/2}=0.95\ . \tag{6.32}$$

This shape parameter is larger than that for the empirical function, so that the latter is bracketed by the last two examples. Substitution of Eq. (6.30) into Eq. (6.15) yields

$$L(z)=\frac{z^2(3-z)}{(1+z)^3}\ln z+z\frac{3z-1}{(1+z)^2}+\frac{\pi z^{3/2}}{(1+z)^3}(1-3z)\ , \tag{6.33}$$

which will be seen to exhibit all of the required properties. It is a straightforward task to extract from Eq. (6.33) the corresponding attenuation function. Although we do not exhibit it here, it is clear from Eq. (6.32) that the midpoint slope of this attenuation function will be less than that of the empirical function.

VII. SUMMARY

In this paper we have tried to paint a detailed picture of the critical behavior of sound propagation near the consolute point of a binary liquid. Carrying the ideas of Laplace,[1] Herzfeld and Rice,[2] Fixman,[4] and Mistura[5] to their logical conclusion, we have established that this critical behavior resides entirely in the relaxational nature of the critical specific heat. We have developed the theory so as to exhibit, at every stage, the dynamic scaling relationship between the applied frequency ω and the intrinsic relaxation rate γ of the fluid. We have made a special effort to establish the model-independent general features of the dependence of the dynamic scaling function on the scaled frequency $\Omega=\omega/\gamma$. Following the treatment of thermodynamics in Sec. II, where we show that the sound velocity is finite at $T=T_c$ and that, near T_c, it has a small critical part which is proportional to C_P^{-1}, we obtain the frequency dependence of the critical-point attenuation in Sec. III. In the more detailed theory of Sec. IV A we have calculated examples of scaling functions from various models. From these examples and guided by some general considerations in Sec. IV B we have extracted the salient model-independent features of the scaling function. In particular, we have found that the scaling function can be accurately characterized by just two parameters—namely, the frequency scale a and the shape parameter b (or alternatively, the shape parameter b'). In this way we were led in Sec. IV C to the empirical function $F(\Omega)=(1+\Omega^{-1/2})^{-2}$, which predicts a linear plot of $\alpha_\lambda^{-1/2}$ versus temperature, in excellent agreement with ex-

periment as shown in Fig. 5, where α_λ is the attenuation per wavelength.

An alternative empirical approach to the scaling function is developed in Sec. VI from a spectral function $f(s)$ that incorporates the Herzfeld-Rice idea of a distribution of relaxing modes contributing to the frequency-dependent specific heat. Like $F(\Omega)$, $f(s)$ is a monotonic function varying smoothly between the zero- and infinite-frequency limits of 0 and 1, respectively. Thus both ways of characterizing the details of the dynamic scaling are similar in that the information is contained in a simple, smooth, positive-definite function. The close connection between $f(s)$ and $F(\Omega)$ is established in Sec. V B by exploiting the analyticity of the scaling function in the complex frequency plane. We show that $f(s)$ versus s has a shape similar to that of $F(\Omega)$ versus Ω, the former being somewhat steeper. Also contained in Sec. V is the dynamic scaling prediction of the theory regarding the sound velocity.

In summary, we believe that the excellent accord that we have found here between the experimental measurements of Garland and Sanchez[17] and the theoretically predicted scaling function, when taken along with the exact agreement established by Clerke *et al.*[9] for the strength of the critical-point attenuation, confirms the dynamic scaling theory of critical ultrasonics in every respect.

ACKNOWLEDGMENTS

It is a pleasure to acknowledge numerous helpful conversations with Professor Carl Garland. This work has been supported by Grants Nos. DMR-79-01172 and DMR-82-05356 from the U. S. National Science Foundation.

APPENDIX A: KAWASAKI FUNCTION

For the $D=D'=3$ one-loop integral, we have used Eq. (4.17) as an approximation to the scaled-pair decay rate

$$\Gamma_3(q)=q^2(1+q^2)^{1/2} . \tag{A1}$$

Here we want to replace Eq. (A1) by the more accurate Kawasaki expression,[24] which we write[25] as $\sigma(q)\Gamma_3(q)$, where

$$\sigma(q)=(1+q^2)^{-1/2}\frac{3}{4q^2}[1+q^2+(q^3-q^{-1})\tan^{-1}q] . \tag{A2}$$

The high- and low-momentum limits are, respectively,

$$\sigma(0)=1 \tag{A3a}$$

and

$$\sigma(\infty)\equiv\sigma_\infty=\frac{3\pi}{8}=1.18 . \tag{A3b}$$

Denoting corrected quantities by a tilde, we find for the one-loop function of Eq. (4.20)

$$\tilde{H}_{33}(z)=\int_0^\infty dq\frac{q^2}{(1+q^2)^2}\frac{\sigma\Gamma_3}{z+\sigma\Gamma_3} . \tag{A4}$$

For $z\gg1$, the high-frequency limit, Eq. (A4) becomes

$$\tilde{H}_{33}(z)=H_{33}(z/\sigma_\infty) . \tag{A5}$$

It follows from Eqs. (4.23), (4.5b), and (A3b) that the corrected frequency-scale parameter is

$$\tilde{a}_{33}=\sigma_\infty a_{33}=1.18a_{33} . \tag{A6}$$

This 18% frequency shift is included in the discussion of Appendix B.

At the low-frequency end of the scale, the dynamics are characterized by the derivative

$$\tilde{H}'_{33}(0)=-\int_0^\infty dq\frac{q^2}{(1+q^2)^2}\frac{\sigma^{-1}}{\Gamma_3}$$
$$=-\int_0^\infty dq(1+q^2)^{-5/2}\sigma^{-1} . \tag{A7}$$

The correction produced by the Kawasaki function is expressed by the ratio

$$\frac{\tilde{H}'_{33}(0)}{H'_{33}(0)}=\langle\sigma^{-1}\rangle , \tag{A8}$$

with the average over momentum space defined by

$$\langle\sigma^{-1}\rangle=\frac{\int_0^\infty dq(1+q^2)^{-5/2}\sigma^{-1}(q)}{\int_0^\infty dq(1+q^2)^{-5/2}} . \tag{A9}$$

In the low-momentum range, $\sigma^{-1}(q)$ is very close to 1. To estimate the average deviation from 1 in Eq. (A8), we can use the first term in the expansion

$$\sigma^{-1}-1=-\frac{q^2}{10}+\cdots \tag{A10}$$

to obtain

$$\langle\sigma^{-1}\rangle-1\simeq-\frac{1}{10}\frac{\int_0^\infty dq\frac{q^2}{(1+q^2)^{-5/2}}}{\int_0^\infty dq(1+q^2)^{-5/2}}=-\frac{1}{20} , \tag{A11}$$

representing a 5% decrease. Including higher terms shows that this is an overestimate of the effect by roughly a factor of 2, with the actual decrease of $\tilde{H}'_{33}(0)$ relative to $H'_{33}(0)$ equaling only 2%. Coupled with the 18% increase in a_{33}, this gives for the shape parameter, according to Eqs. (4.6) and (4.35e),

$$\tilde{b}_{33}=1.16b_{33}=1.16\times9.29=10.8 . \tag{A12}$$

This is close to the value $b=11.6$ found in Eq. (4.75) for the empirical function, which gives further support to the latter as being a faithful representation of the theoretically predicted attenuation function.

APPENDIX B: ϵ EXPANSION

Here we investigate the feasibility of determining the frequency-scale parameter a by an expansion in powers of $\epsilon=4-D$. This study is necessitated by the fact that the graph shown in Fig. 3(c) has to be evaluated in the ϵ expansion. The single-loop integral in D dimensions with a critical slowing down expressed by $\Gamma(k)\sim k^{D'}$ yields Eq. (4.28), which can be rewritten as

$$\frac{1}{D'}\ln a_{DD'}=\frac{1}{\epsilon}\ln\left[\frac{2}{D'}\frac{1}{1-\epsilon/2}\frac{\sin(\pi\epsilon/2)}{\sin(\pi\epsilon/D')}\right]. \quad \text{(B1)}$$

Equations (4.30a)—(4.30h) give the values of $a_{DD'}$ that result from Eq. (B1) by setting ϵ equal to 0, 1, and 2, while choosing various integer values for D'. This straightforward procedure has the merit of simplicity, but the disadvantage that, by choosing integer values of ϵ, it is difficult to compare the resulting changes in $\ln a$ with the change $(\Delta \ln a)_{\rm hydro}$ resulting from the coupling to the transverse hydrodynamic modes, as illustrated in Fig. 3(c). The computation[27] of this effect, which is carried out to the lowest order in the ϵ expansion, yields

$$(\Delta \ln a)_{\rm hydro}=-\frac{\pi^2}{12}\epsilon\ . \quad \text{(B2)}$$

In order to obtain an estimate of the reliability of this low-order result, it is useful to study the corresponding first-order expansion of Eq. (B1) for an arbitrary value of D',

$$\frac{1}{D'}\ln a_{DD'}\simeq\tfrac{1}{2}-\left[\pi^2\left[\frac{1}{24}-\frac{1}{D'^2}\right]-\frac{1}{8}\right]\epsilon\ . \quad \text{(B3)}$$

This low-order expansion can be tested for $\epsilon=1$ and $D'=4$, 3, and 2 by examining

$$(\Delta \ln a)_{DD'}\equiv\ln a_{DD'}-\ln a_{44}\ . \quad \text{(B4)}$$

Equation (B3) gives

$$(\Delta \ln a)_{34}=-0.73\ , \quad \text{(B5a)}$$

$$(\Delta \ln a)_{33}=-0.81\ , \quad \text{(B5b)}$$

and

$$(\Delta \ln a)_{32}=-0.75\ , \quad \text{(B5c)}$$

while, from Eqs. (4.30d)—(4.30f), the exact values are

$$(\Delta \ln a)_{34}=-0.61\ , \quad \text{(B6a)}$$

$$(\Delta \ln a)_{33}=-0.70\ , \quad \text{(B6b)}$$

and

$$(\Delta \ln a)_{32}=-0.61\ . \quad \text{(B6c)}$$

The error in Eqs. (B5a)—(B5c) of the order of 20%, is acceptable for such a low-order truncation. This satisfactory performance of the ϵ expansion worsens, however, when it is extended to a simultaneous expansion in powers of $\epsilon'=4-D'$. To first order in ϵ', Eqs. (B3) and (B4) become

$$(\Delta \ln a)_{DD'}=-\left[\frac{\pi^2}{8}-\tfrac{1}{2}\right]\epsilon-\tfrac{1}{2}\epsilon'\ . \quad \text{(B7)}$$

For $\epsilon=1$ and $\epsilon'=2$, Eq. (B7) would give

$$(\Delta \ln a)_{32}=-1.73\ , \quad \text{(B8)}$$

which, by comparing with Eq. (B6c), is obviously grossly in error. This reflects the neglect of the onset of the infrared divergence at $D=D'=2$ that was noted in Sec. IV in connection with Eqs. (4.30g) and (4.30h). We have found[28] that such an infrared divergence is quite common in critical dynamics and that the neglect of it is generally the principal source of inaccuracy in the ϵ expansion. The error is evidently already serious for the $D=D'=3$ case. Setting $\epsilon'=\epsilon$ in Eq. (B7) gives

$$(\Delta \ln a)_{\text{one-loop}}=-\frac{\pi^2}{8}\epsilon\ , \quad \text{(B9)}$$

or $-\pi^2/8=-1.23$ for $\epsilon=1$. Thus, the first-order ϵ expansion overestimates the one-loop integral by the factor $1.73/0.71=1.75=\frac{7}{4}$. In other words, the first-order ϵ expansion requires the correction factor $\frac{4}{7}$. Our study of the hydrodynamic effect that is illustrated in Fig. 3(c), and which yields Eq. (B2), indicates that it also has an infrared divergence. It follows that Eq. (B2) is also an overestimate because it, too, takes no account of this incipient divergence. Therefore, Eq. (B2) requires a correction factor similar to that required for the ϵ expansion of the one-loop integral. In the absence of more detailed information, we adopt the working hypothesis that the two correction factors are equal (or approximately so). This implies that Eq. (B2) should also be reduced by $\frac{4}{7}$.

An equivalent, alternative approach for correcting the ϵ-expansion error in Eq. (B2) is to note the following simple ratio between the ϵ-expansion results in Eqs. (B2) and (B9):

$$\frac{(\Delta \ln a)_{\rm hydro}}{(\Delta \ln a)_{\text{one-loop}}}=\frac{2}{3}\ . \quad \text{(B10)}$$

Therefore, the total change in $\ln a$ is

$$\begin{aligned}(\Delta \ln a)_{\rm tot}&=(\Delta \ln a)_{\text{one-loop}}+(\Delta \ln a)_{\rm hydro}\\&=\left[1+\frac{(\Delta \ln a)_{\rm hydro}}{(\Delta \ln a)_{\text{one-loop}}}\right](\Delta \ln a)_{\text{one-loop}}\\&=\tfrac{5}{3}(\Delta \ln a)_{\text{one-loop}}\ . \end{aligned} \quad \text{(B11)}$$

At this stage we replace the ϵ-expansion value of $(\Delta \ln a)_{\text{one-loop}}$ by its true value, as given by Eq. (B6b), to obtain

$$\ln a=2-\tfrac{5}{3}(0.71)=0.82\ . \quad \text{(B12)}$$

Including the 18% high-frequency correction from the Kawasaki function, as discussed in Appendix A, gives

$$a=\frac{3\pi}{8}e^{0.82}=2.67\ . \quad \text{(B13)}$$

Substituting Eq. (4.73) then yields

$$\Omega_{1/2}=0.79a=2.1\ . \quad \text{(B14)}$$

This result is in good agreement with the experimental value of 2.0 that is shown by the dashed line in Fig. 7.

It would take us too far afield to discuss b, the other parameter of the problem. In a separate publication[27] we will show that the shape parameter is modified only very little by the hydrodynamic coupling, thereby, justifying the use of the one-loop integrals and the closely related empirical attenuation function.

[1]P. S. LaPlace, Ann. Chim. Phys. Tome iii, 238 (1816).
[2]K. E. Herzfeld and F. O. Rice, Phys. Rev. **31**, 691 (1928).
[3]A. B. Bhatia, *Ultrasonic Attenuation* (Oxford University, London, 1967).
[4]M. Fixman, J. Chem. Phys. **36**, 1961 (1962).
[5]L. Mistura, in *Proceedings of the Varenna Summer School on Critical Phenomena,* edited by M. S. Green (Academic, New York, 1971).
[6]R. A. Ferrell and J. K. Bhattacharjee, Phys. Lett. **86A**, 109 (1981).
[7]R. A. Ferrell and J. K. Bhattacharjee, Phys. Rev. Lett. **44**, 403 (1980); Phys. Rev. B **23**, 2434 (1981).
[8]J. K. Bhattacharjee and R. A. Ferrell (unpublished).
[9]E. A. Clerke, J. V. Sengers, R. A. Ferrell, and J. K. Bhattacharjee, Phys. Rev. A **27**, 2140 (1983).
[10]E. A. Clerke, Ph.D. thesis, Department of Physics and Astronomy, University of Maryland, College Park, Maryland, 1982.
[11]Y. Harada, Y. Suzuki, and Y. Ishida, J. Phys. Soc. Jpn. **48**, 703 (1980); see also Y. Ishida and Y. Harada, Jpn. J. Appl. Phys. **19**, 1563 (1980).
[12]K. Kawasaki, Phys. Rev. A **1**, 1750 (1970).
[13]Y. Shiwa and K. Kawasaki, Prog. Theor. Phys. **66**, 406 (1981).
[14]D. M. Kroll and J. M. Ruhland, Phys. Lett. **80A**, 45 (1980).
[15]For a discussion of the second viscosity coefficient in the present context, see Sec. II.30 of K. F. Herzfeld and T. A. Litovitz, *Absorption and Dispersion of Ultrasonic Waves* (Academic, New York, 1959).
[16]J. K. Bhattacharjee and R. A. Ferrell, Phys. Rev. A **24**, 1643 (1981).
[17]C. W. Garland and G. Sanchez, J. Chem. Phys. **79**, 3090 (1983); see also G. Sanchez and C. W. Garland, *ibid.* **79**, 3100 (1983).
[18]D. Beysens and R. Tufeu, Rev. Phys. Appl. **14**, 907 (1979).
[19]R. A. Ferrell and J. K. Bhattacharjee, Phys. Rev. B **24**, 4095 (1981).
[20]G. Ahlers, Phys. Rev. **182**, 352 (1969).
[21]R. A. Ferrell and J. K. Bhattacharjee, Phys. Rev. B **25**, 3168 (1982).
[22]H. Tanaka, Y. Wada, and H. Nakajima, Chem. Phys. **68**, 223 (1982); **75**, 37 (1983).
[23]M. Barmatz and I. Rudnick, Phys. Rev. **170**, 224 (1968).
[24]K. Kawasaki, Ann. Phys. (N.Y.) **61**, 1 (1970).
[25]R. A. Ferrell, Phys. Rev. Lett. **24**, 1169 (1970).
[26]M. E. Fisher and J. S. Langer, Phys. Rev. Lett. **20**, 665 (1968).
[27]J. K. Bhattacharjee and R. A. Ferrell (unpublished).
[28]J. K. Bhattacharjee and R. A. Ferrell, J. Math. Phys. **21**, 534 (1980); see also Phys. Rev. A **28**, 2363 (1983).